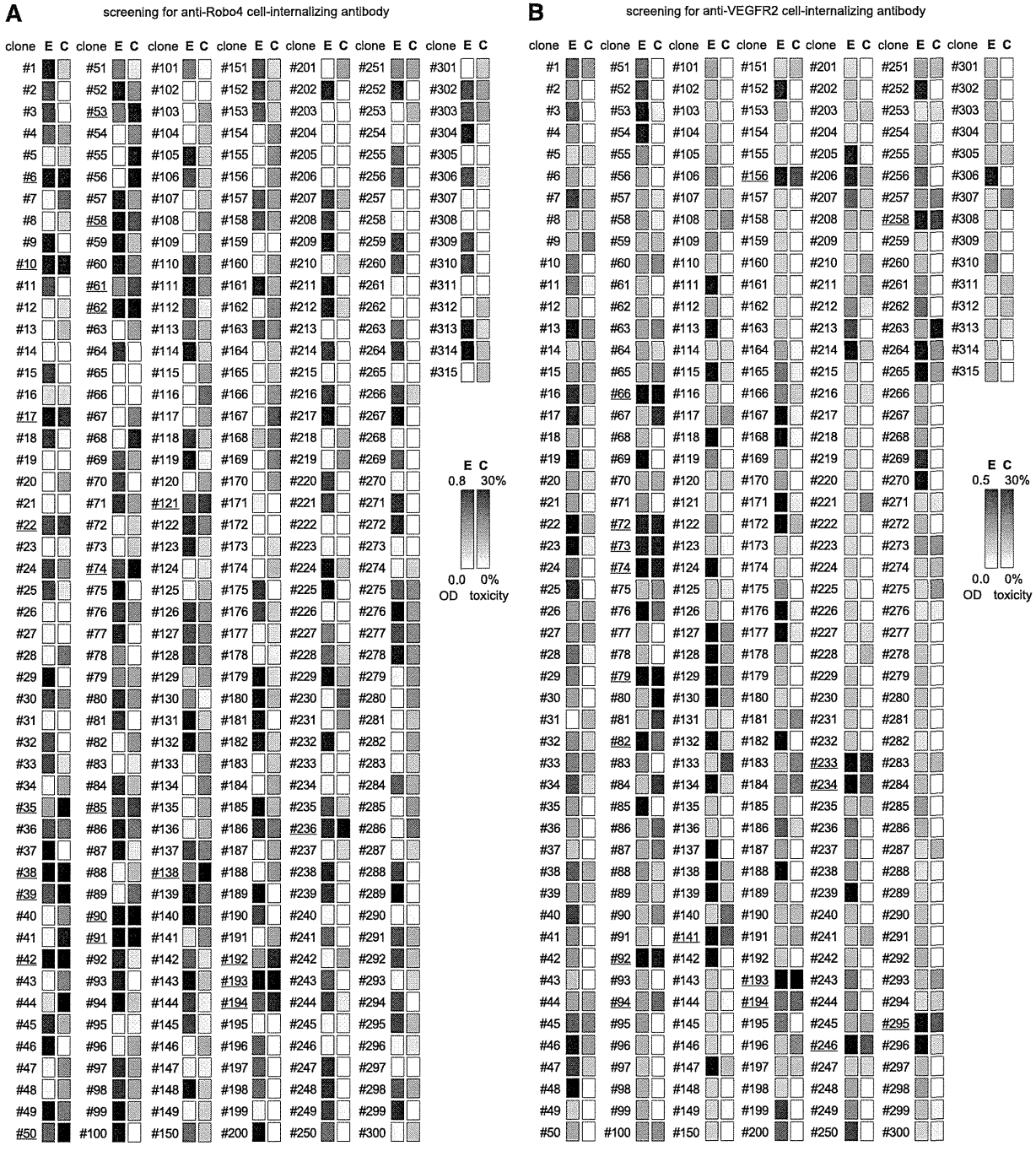

Figure 2. Screening of cell-internalizing mAbs (ELISA and cytotoxicity assay). To screen for cell-internalizing mAbs, 315 clones per antigen were analyzed by ELISA and cytotoxicity assay. (A) Result for Robo4, (B) Result for VEGFR2. Monoclonal scfv-PSIFs were induced in TG1 supernatant. The binding properties and cytotoxicities to MS1 cells were then assessed by an ELISA and WST-8 assay, respectively. E, ELISA results; C, WST-8 assay results. Individual results from ELISA (OD = 0.8 or 0.5~0.0) and WST-8 assay (cytotoxicity = 30%~0%) were mapped in grayscale densities. The 24 candidates against Robo4 and 17 candidates against VEGFR2 are indicated by the underline (ELISA OD ≥0.2 and cytotoxicity ≥20%). After omitting redundant clones by sequencing, 1 cell-internalizing mAb and 2 low-internalizing mAbs against mRobo4, and 2 cell-internalizing mAbs and 14 low-internalizing mAbs against mVEGFR2 were identified.

(Figure 2A). In a similar manner, for anti-VEGFR2s, 156 of 315 clones bound to VEGFR2 and 17 of the 156 binders were positive in the ELISA and cytotoxicity assays (Figure 2B). Sequence analysis to omit redundant clones revealed that these clones comprised 1 anti-Robo4 cell-internalizing mAb, 2 anti-Robo4 low-internalizing mAbs, 2 anti-VEGFR2 cell-internalizing mAbs, and 14 anti-VEGFR2 low-internalizing mAbs. For anti-Robo4s, only one anti-Robo4 cell-internalizing mAb was named "R4-13i" and a low-internalizing mAb with high affinity and low cytotoxicity was named "R4-16." In a similar manner, "V2-05i" and "V2-02" were selected as an anti-VEGFR2 cell-internalizing mAb and a low-internalizing mAb, respectively. After purification of the recombinant proteins, both anti-Robo4 scFvs bound to hRobo4, similar to mRobo4. Conversely, anti-VEGFR2 scFvs bound to

Table 1. Binding kinetics of antibodies in surface plasmon resonance analysis

Antibody	Target	Format	k_a ($M^{-1}s^{-1}$)	k_d (s^{-1})	K_D (M)
R4-13i	mRobo4	scFv	$1.25 \pm 0.36 \times 10^5$	$5.82 \pm 0.95 \times 10^{-4}$	$5.03 \pm 1.95 \times 10^{-9}$
(internalizing)		dscFv	$1.15 \pm 0.34 \times 10^6$	$5.98 \pm 0.61 \times 10^{-4}$	$5.64 \pm 2.21 \times 10^{-10}$
		IgG	$1.14 \pm 0.55 \times 10^6$	$4.19 \pm 1.70 \times 10^{-4}$	$2.22 \pm 0.51 \times 10^{-10}$
		scFv-PSIF	$7.22 \pm 4.31 \times 10^4$	$4.28 \pm 1.60 \times 10^{-3}$	$6.47 \pm 1.61 \times 10^{-8}$
		IgG-NCS	$1.02 \pm 0.15 \times 10^6$	$4.66 \pm 0.86 \times 10^{-4}$	$4.59 \pm 0.74 \times 10^{-10}$
R4-16	mRobo4	scFv	$1.30 \pm 0.33 \times 10^5$	$5.82 \pm 1.50 \times 10^{-4}$	$4.77 \pm 1.96 \times 10^{-9}$
(low-internalizing)		dscFv	$1.12 \pm 0.03 \times 10^6$	$5.91 \pm 1.50 \times 10^{-4}$	$5.31 \pm 1.96 \times 10^{-10}$
		IgG	$1.06 \pm 0.24 \times 10^6$	$3.60 \pm 0.85 \times 10^{-4}$	$2.76 \pm 0.16 \times 10^{-10}$
		scFv-PSIF	$8.90 \pm 1.42 \times 10^4$	$6.10 \pm 2.45 \times 10^{-3}$	$7.24 \pm 3.74 \times 10^{-8}$
		IgG-NCS	$1.07 \pm 0.12 \times 10^6$	$3.93 \pm 0.54 \times 10^{-4}$	$3.72 \pm 0.89 \times 10^{-10}$
V2-05i	mVEGFR2	scFv	$9.66 \pm 3.57 \times 10^4$	$4.40 \pm 0.95 \times 10^{-4}$	$5.13 \pm 2.61 \times 10^{-9}$
(internalizing)		dscFv	$8.75 \pm 2.03 \times 10^5$	$5.59 \pm 2.57 \times 10^{-4}$	$6.16 \pm 1.47 \times 10^{-10}$
		IgG	$1.14 \pm 0.09 \times 10^6$	$3.21 \pm 0.35 \times 10^{-4}$	$2.84 \pm 0.52 \times 10^{-10}$
		scFv-PSIF	$9.57 \pm 0.84 \times 10^4$	$6.51 \pm 1.87 \times 10^{-3}$	$6.94 \pm 2.63 \times 10^{-8}$
		IgG-NCS	$0.96 \pm 0.06 \times 10^6$	$4.37 \pm 0.90 \times 10^{-4}$	$4.52 \pm 0.79 \times 10^{-10}$
V2-02	mVEGFR2	scFv	$7.94 \pm 1.24 \times 10^4$	$4.28 \pm 3.23 \times 10^{-4}$	$5.07 \pm 3.05 \times 10^{-9}$
(low-internalizing)		dscFv	$8.94 \pm 2.55 \times 10^5$	$5.57 \pm 1.25 \times 10^{-4}$	$6.60 \pm 2.39 \times 10^{-10}$
		IgG	$1.13 \pm 0.22 \times 10^6$	$3.25 \pm 1.10 \times 10^{-4}$	$2.90 \pm 0.98 \times 10^{-10}$
		scFv-PSIF	$9.84 \pm 1.52 \times 10^4$	$5.75 \pm 2.05 \times 10^{-3}$	$5.81 \pm 1.93 \times 10^{-8}$
		IgG-NCS	$1.08 \pm 0.08 \times 10^6$	$5.25 \pm 1.58 \times 10^{-4}$	$4.85 \pm 1.30 \times 10^{-10}$

Binding kinetics were analyzed against mRobo4 (R4-13i and R4-16) or mVEGFR2 (V2-05i and V2-02). Values are shown as means ± SD from three different preparations.

k_a, association rate constant ($M^{-1}s^{-1}$); k_d, dissociation rate constant (s^{-1}); K_D, equilibrium dissociation constant (k_d/k_a) (M).

mVEGFR2, but not to hVEGFR2. We also confirmed using competitive ELISA that the mAbs did not share their antigen-binding epitopes (supplemental Figure 2).

Characterization of mAbs

We purified scFvs, dimerized scFvs (dscFvs), IgGs, and scFv-PSIF as recombinant proteins. IgGs conjugated with neocarzinostatin (IgG-NCSes) were also prepared for in vivo experiments. NCSes were confirmed to be conjugated to IgG molecules in the purified IgG-NCS fraction, and the efficiencies of the NCS modifications were similar in all IgG-NCSes (1.6~1.8 NCSes per single IgG). Surface plasmon resonance analysis revealed that cell-internalizing mAbs and low-internalizing mAbs had similar affinities against antigens in all antibody forms (Table 1).

To quantify the internalization, flow cytometry analysis was performed with Cy5.5-labeled mAbs ($scFv^{Cy5.5}$, $dscFv^{Cy5.5}$, and $IgG^{Cy5.5}$; Figure 3A,C). After $mAbs^{Cy5.5}$ bound to the cell surface, internalization was induced by incubation at 37°C for 2 hours. By removing cell-surface $mAbs^{Cy5.5}$ with trypsinization, the internalized $mAbs^{Cy5.5}$ were quantified by flow cytometry. At 2 hours, approximately 30% of cell-internalizing mAbs remained after trypsinization, whereas most of the low-internalizing mAbs were degraded (Figure 3A,C). This result clearly suggested that the internalization efficiencies differed between cell-internalizing mAbs and low-internalizing mAbs, even among the three different mAb forms. In a similar manner, a time-shift analysis revealed that >40% of cell-internalizing mAbs were internalized after 8 hours of incubation (Figure 3B,D). These findings indicate that only cell-internalizing mAbs were efficiently internalized into the cells, although low-internalizing mAbs had affinities similar to those of cell-internalizing mAbs (Table 1).

Intracellular localization

The intracellular behaviors of cell-internalizing mAbs were analyzed with a confocal laser-scanning microscope. In MS1 cells, intracellular fluorescence derived from $scFv^{Cy5.5}$ was observed with cell-internalizing scFvs, but not with low-internalizing scFvs (supplemental Figure 3A,D,E,H). Fluorescence was suppressed, however, under the inhibition of energy-dependent endocytosis (supplemental Figure 3B-C,F-G). These results suggested that cell-internalizing scFvs entered into the cells via energy-dependent endocytosis.

For in-depth analysis of the intracellular behavior, confocal laser-scanning microscope analysis was performed with immunostaining of endosome markers (supplemental Figure 3Iab). After $scFvs^{Cy5.5}$ were bound to the cell-surface, the cells were incubated for an additional 1 to 8 hours at 37°C. The early endosome marker, early endosome antigen 1 (EEA1), and the late endosome marker, lysosomal-associated membrane protein 1 (LAMP1), were visualized using Alexa488-conjugated antibodies. Colocalization with EEA1+ early endosomes decreased over time (supplemental Figure 3I-M,S-W), whereas colocalization with LAMP1+ late endosomes increased (supplemental Figure 3N-R,Xab). These findings suggested that cell-internalizing scFvs were encapsulated in EEA1+ early endosomes at an early stage and eventually accumulated in LAMP1+ late endosomes. This is thought to be a typical endocytotic molecular sorting pathway.[39]

Influence of cell-internalizing activity on biodistribution

To assess the biodistribution of cell-internalizing mAbs, ^{125}I-labeled dscFvs ($dscFv^{125I}$) were intravenously injected into B16BL6 tumor-bearing mice. In this experiment, we selected the dscFv form because dscFv has superior in vivo tumor-targeting potency compared with scFv.[40] At 2 hours, the tumor distribution of anti-Robo4 and anti-VEGFR2 $dscFvs^{125I}$ was similar to but significantly higher than that of a negative control $dscFv^{125I}$ ($anti\text{-}His[dscFv]^{125I}$; Figure 4A-B). This finding suggested that the anti-Robo4 and anti-VEGFR2 dscFvs had tumor-targeting properties. Anti-Robo4 $dscFvs^{125I}$ also accumulated in the kidney, indicating a nonspecific distribution of dscFvs for their elimination,[41,42] because no significant difference was observed between anti-Robo4 $dscFvs^{125I}$

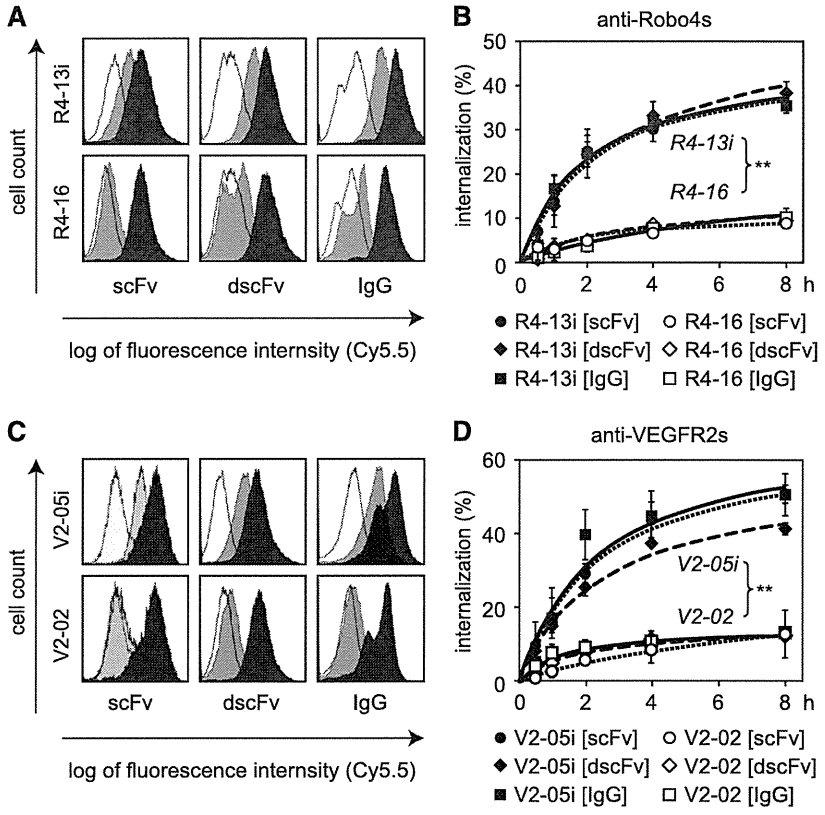

Figure 3. Cell internalization analyzed by flow cytometry. (A,C) Trypsinization to quantify internalized mAbs. Different forms of $mAbs^{Cy5.5}$ bound to the MS1 cells at 4°C. After washing out the unbound mAbs, internalization was induced for 2 hours at 37°C. To detect only internalized mAbs, cell surface proteins were trypsinized. The remaining cellular fluorescence was then analyzed by flow cytometry. (A) Anti-Robo4 $mAbs^{Cy5.5}$, (C) Anti-VEGFR2 $mAbs^{Cy5.5}$. Black, nontrypsinized group; gray, trypsinized group; white, negative control (anti-His[scFv]$^{Cy5.5}$, anti-His[dscFv]$^{Cy5.5}$, or anti-FLAG [IgG]$^{Cy5.5}$). (B,D) Time course of the internalization. After binding at 4°C, internalization was induced for 0.5, 1, 2, 4, or 8 hours at 37°C. The ratio of internalization was calculated using the following formula: internalization (%) = {internalized mAb}/{total bound mAb} × 100 (%) = {(MFI of mAb)$_T$ − (MFI of negative control)$_T$}/{(MFI of mAb)$_N$ − (MFI of negative control)$_N$} × 100 (%). T, trypsinized group; N, nontrypsinized group; MFI, mean fluorescence intensity. (B) Closed and open markers indicate R4-13i and R4-16, respectively. (D) Closed and open markers indicate V2-05i and V2-02, respectively. (B,D) Circles, diamonds, and squares indicate scFv, dscFv, and IgG, respectively. Each experiment was performed in triplicate. Values are shown as means ± SD. $^{**}P < .01$; internalizing mAb versus low-internalizing mAb in each form by 2-way ANOVA (n = 3).

and anti-His[dscFv]^{125I} (Figure 4A). Importantly, the accumulation of anti-VEGFR2 $dscFvs^{125I}$ in the kidney was significantly greater than that of anti-His[dscFv]^{125I} (Figure 4B). A similar accumulation of anti-VEGFR2 $dscFvs^{125I}$, but not anti-Robo4 $dscFvs^{125I}$ (Figure 4A), was observed in the heart (Figure 4B).

To confirm this phenomenon, the localization of dscFvs in the tissues was analyzed by immunofluorescence studies (Figure 4E-S). Biotin-labeled dscFvs ($dscFvs^{Bio}$) were intravenously administered to B16BL6 tumor–bearing mice and the tumors, kidneys, and hearts were extracted 2 hours after injection. The $dscFv^{Bio}$ and vascular endothelial cells were stained by streptavidin-AP and anti-CD31 antibody, respectively. In the tumor sections, all of the anti-Robo4 and anti-VEGFR2 $dscFvs^{Bio}$ were clearly detected with CD31+ tumor blood vasculature, whereas anti-His[dscFv]^{Bio} was not detectable (Figure 4E,H,K,N,Q). This finding suggested that both anti-Robo4 and anti-VEGFR2 dscFvs recognized tumor endothelial cells in vivo, which contributed to their accumulation in the tumor. Interestingly, in the kidney and heart sections, signals around CD31+ blood vasculature were detectable only with the anti-VEGFR2 $dscFvs^{Bio}$, and not with anti-Robo4 $dscFvs^{Bio}$ or anti-His[dscFv]^{Bio} (Figure 4F-G,I-J,L-M,O-P,R-S). This finding was compatible with the biodistribution results (Figure 4A-B), which suggested that anti-VEGFR2 dscFvs recognized VEGFR2 on normal blood vessels because VEGFR2 plays an important role in normal tissues, including the kidney and heart.[31-33] No specific accumulation of anti-Robo4 dscFvs was observed in normal tissues, suggesting that the anti-Robo4 mAbs were useful for specific tumor vascular targeting.

Comparison of the cell-internalizing mAbs and low-internalizing mAbs revealed a significantly greater accumulation of cell-internalizing $dscFvs^{125I}$ in the tumors compared with low-internalizing $dscFvs^{125I}$ at 24 hours (Figure 4C-D), whereas no differences were observed at 2 hours (Figure 4A-B). This finding suggested that cell-internalizing mAbs were retained in the tumor for a longer time than the low-internalizing mAbs. This phenomenon was also observed in the kidney and heart with the anti-VEGFR2 dscFvs (Figure 4D). This retention might be caused by the mAb internalization, which allowed the mAb to escape from the bloodstream and accumulate in the tumor blood endothelial cells. Taken together, these results suggest that mAb internalization into the tumor endothelium improves mAb-based drug-delivery in vivo.

Enhanced antitumor effect depends on the cell-internalizing activity

To assess the antitumor potencies of the cell-internalizing mAbs, we selected the scFv-PSIF and IgG-NCS forms. Both forms were suitable models of ADCs because both drugs are used clinically as successful anticancer medicines.[10,43] First, the in vitro cell-killing activities of scFv-PSIFs and IgG-NCSes were estimated by a cytotoxicity assay with MS1 cells (Figure 5A-D). Both forms of cell-internalizing mAbs showed an approximately 10-fold higher cytotoxicity than the low-internalizing mAbs. These findings clearly suggest that internalization enhanced the delivery of conjugated drugs into the cells because our cell-internalizing mAbs and low-internalizing mAbs had similar affinities against antigens (Table 1).

As the therapy experiment in vivo, scFv-PSIFs and IgG-NCSes were intravenously injected into B16BL6 tumor–bearing mice once every 2 days for a total of 5 injections (Figure 5E-H). All cell-internalizing mAbs significantly suppressed tumor growth, whereas the antitumor effects of the low-internalizing antibodies were

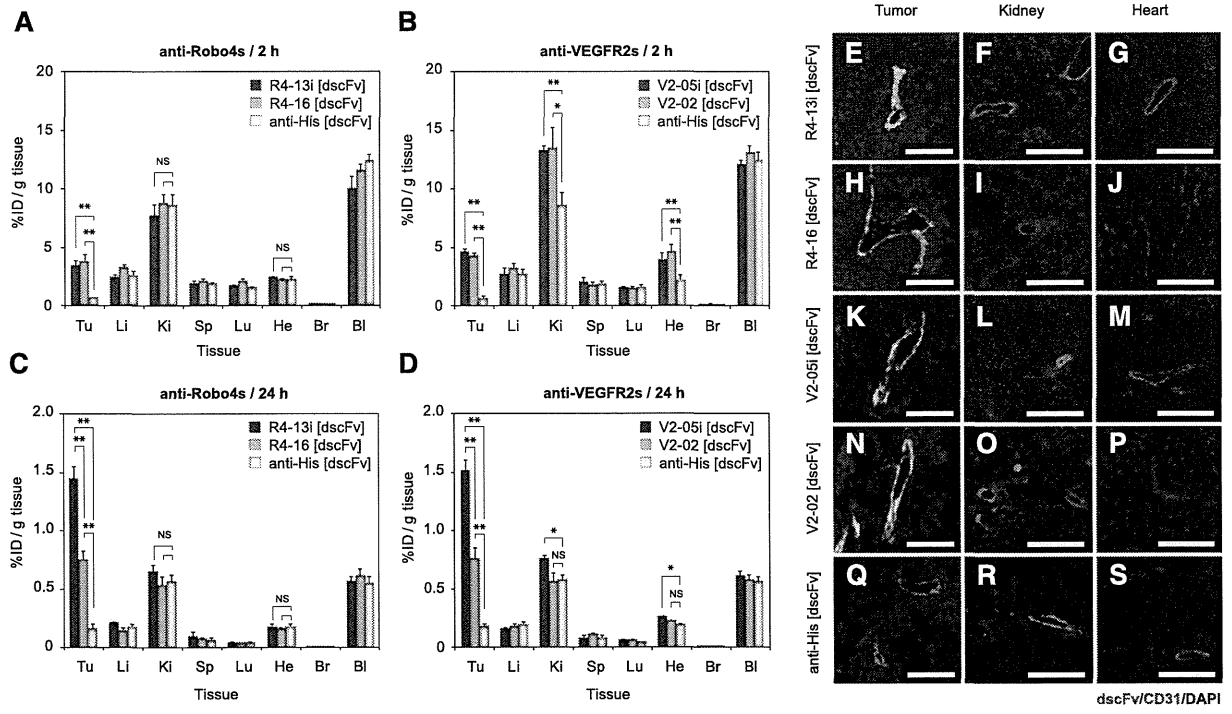

Figure 4. In vivo tumor-targeting activity of cell-internalizing mAbs. (A-D) Biodistribution of dscFvs in B16BL6 tumor–bearing mice. B16BL6 tumor–bearing mice were intravenously administered with anti-Robo4 dscFvs^{125I} (A,C) or anti-VEGFR2 dscFvs^{125I} (B,D). Each organ was extracted after 2 hours (A,B) or 24 hours (C,D), and the radioactivity was measured using a γ counter. %ID/g tissue was calculated using the following formula: %ID/g tissue = (count/g tissue)/(total injected count) × 100 (%). Tu, tumor; Li, liver; Ki, kidney; Sp, spleen; Lu, lung; He, heart; Br, brain; Bl, blood. (A,C) black; R4-13i[dscFv]^{125I}; gray, R4-16[dscFv]^{125I}; white, anti-His[dscFv]^{125I}. (B,D) black, V2-05i[dscFv]^{125I}; gray, V2-02[dscFv]^{125I}; white, anti-His[dscFv]^{125I}. Values are shown as means ± SEM. $^*P < .05$; $^{**}P < 0.01$; NS, not significant in Student's *t*-test (n = 11). (E-S) Co-immunostaining of dscFvs with CD31$^+$ blood endothelial cells on the tissue section. B16BL6 tumor–bearing mice were intravenously administered dscFvs^{Bio}. The tumor, kidney, and heart were extracted after 2 hours. Tissue sections of tumor, kidney, and heart were stained with streptavidin-PE conjugate. The blood vasculature was also stained with anti-CD31 antibody. Images were digitally merged. Red, dscFv^{Bio}; green, CD31; blue, DAPI (nucleus); yellow, colocalized region of red and green. Scale bar represents 100 μm. (E-G) R4-13i[dscFv]; (H-J) R4-16[dscFv]; (K-M) V2-05i[dscFv]; (N-P) V2-02[dscFv]; (Q-S) anti-His[dscFv]. (E,H,K,N,Q) Tumor section, (F,I,L,O,R) kidney section, and (G,J,M,P,S) heart section.

similar to those of the negative controls (anti-His[scFv]-PSIF and anti-FLAG[IgG]-NCS). The antitumor effects of R4-13i and V2-05i were similar in both ADC forms. These findings strongly suggest that the cell-internalizing activity of the mAbs was essential to maximize the delivery of the conjugated drug into the target cells, which significantly enhanced the antitumor effect of the ADCs.

Interestingly, the group of mice administered V2-05i[scFv]-PSIF had a significant loss of body weight, whereas the other groups did not (Figure 5I-L). As a preliminary result, 6 of 7 mice died in the V2-05i[scFv]-PSIF group with a similar protocol but with a fourfold higher dosage (60 pmol/mouse), perhaps because of the disruption of VEGFR2-positive cells in normal tissues by V2-05i[scFv]-PSIF, as shown in Figure 4. This side effect was not observed in the V2-05i [IgG]-NCS group. Therefore, we also hypothesized that the toxicity of NCS in normal cells was weak because NCS inhibits DNA synthesis in growing cells, such as tumor cells.[44] At a higher dosage, however, V2-05i[IgG]-NCS carries the risk of side effects. With regard to this point, none of the anti-Robo4 ADCs induced a loss of body weight; therefore, we concluded that Robo4 is a potential target for tumor vascular targeting with ADC.

Discussion

This study led to three novel findings. First, we demonstrated a rapid screening system for cell-internalizing mAbs in combination with the phage antibody library, which accelerated the identification of desired cell-internalizing mAbs. Second, comparative in vivo studies using cell-internalizing mAbs and low-internalizing mAbs with the same affinity values revealed that mAb internalization contributed to tumor targeting and enhanced the antitumor effects of the ADCs. Third, the first in vivo therapeutic application with anti-Robo4 mAb revealed that Robo4 is a therapeutic target on the tumor endothelial cells. The first and second findings will greatly contribute to the development of antibody therapies based on cell-internalizing antibodies such as ADCs, targeted liposomal drugs, or imaging. The third finding provides a new focus regarding the role of Robo4 biology in the body, such as the decreased side effects associated with depleting Robo4-positive endothelial cells in vivo.

This method allowed us to successfully isolate anti-Robo4 and anti-VEGFR2 cell-internalizing mAbs in combination with a phage antibody library and a PSIF-based screening system. This method provided one-step screening of cell-internalization of hundreds of "monoclonal" candidates. This is the main advantage of the present system over the old screening system, which required handling a "polyclonal" pool of mAbs.[6,7] The innovative feature of our method is the use of PSIF as a fusion partner for antibodies in scFv format, thus facilitating the identification of antibody fragments capable of efficient internalization. The scFv fusion is much easier than the chemical conjugation of the antibody to a cytotoxic drug. In principle, this method can be applied to other phage libraries, such as nonimmune phage antibody libraries[35,45] or synthetic

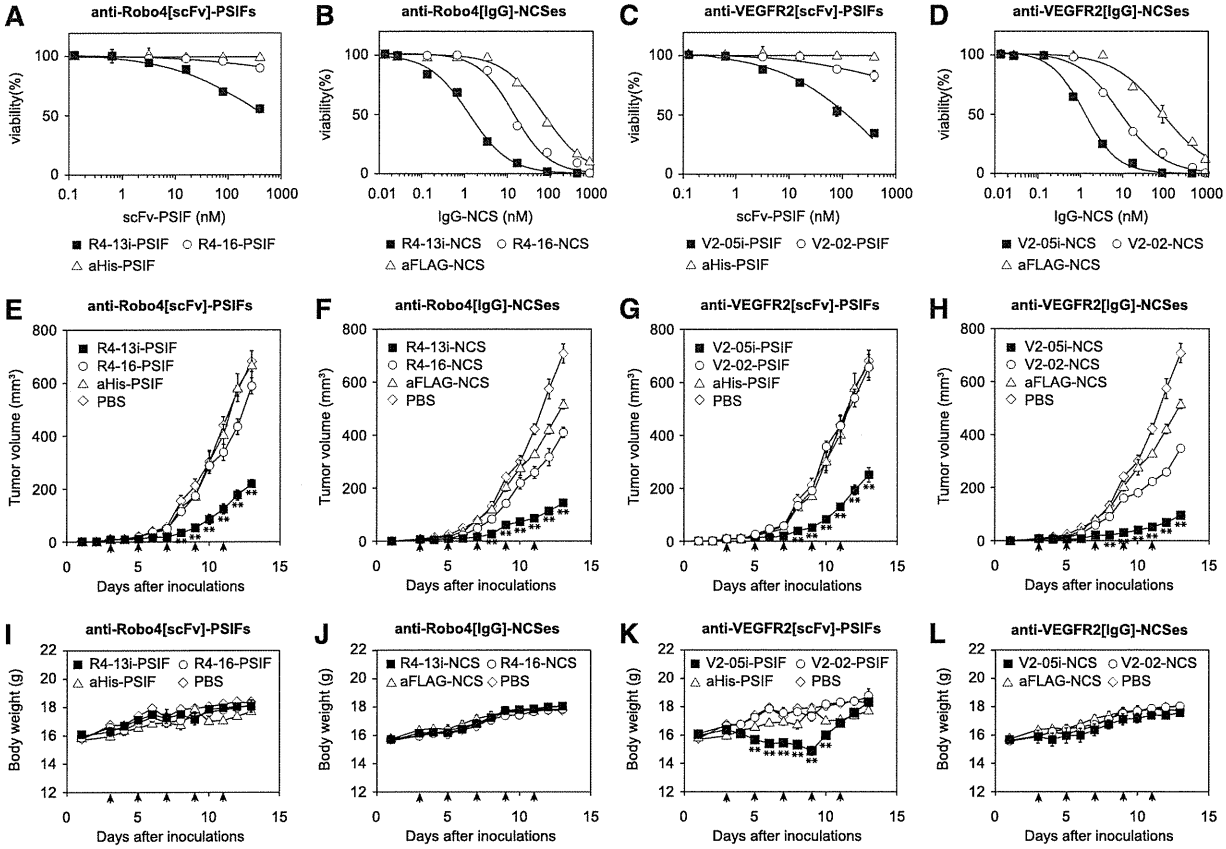

Figure 5. Enhanced anti-tumor effect of cell-internalizing mAbs. (A-D) Cytotoxicity of scFv-PSIF and IgG-NCS against MS1 cells. MS1 cells were incubated with serially diluted mAb-drug conjugates for 24 hours. Cell viability was then measured using a WST-8 assay. Closed square, internalizing mAbs; open circle, low-internalizing mAbs; open triangle, negative controls. (A) anti-Robo4[scFv]-PSIFs, (B) anti-Robo4[IgG]-NCSes, (C) anti-VEGFR2[scFv]-PSIFs, (D) anti-VEGFR2[IgG]-NCSes. Anti-His[scFv]-PSIF and anti-FLAG[IgG]-NCS were used as negative controls. Values are shown as means ± SD. (E-H) Antitumor effects of scFv-PSIFs or IgG-NCSes. B16BL6 cells were inoculated intracutaneously into C57BL6 mice on day 0. On days 3, 5, 7, 9, and 11, mAb-drug conjugates were intravenously administered *(arrow heads)*. Tumor volume was calculated using the following formula: tumor volume (mm^3) = {major axis of tumor (mm)} × {minor axis of tumor (mm)}^{2} × 0.4. Closed square, internalizing mAbs; open circle, low-internalizing mAbs; open triangle, negative controls (anti-His[scFv]-PSIF or anti-FLAG[IgG]-NCS); open diamond, PBS. (E) Anti-Robo4[scFv]-PSIFs, (F) anti-Robo4[IgG]-NCSes, (G) anti-VEGFR2[scFv]-PSIFs, (H) anti-VEGFR2[IgG]-NCSes. Values are shown as means ± SEM. $^{**}P < 0.01$; internalizing mAbs versus low-internalizing mAbs by Bonferroni post hoc analysis with two-way ANOVA (n = 6). (I-L) Change in body weight during therapy experiment. Closed square, internalizing mAbs; open circle, low-internalizing mAbs; open triangle, negative controls (anti-His[scFv]-PSIF or anti-FLAG[IgG]-NCS); open diamond, PBS. (I) anti-Robo4[scFv]-PSIFs, (J) anti-Robo4[IgG]-NCSes, (K) anti-VEGFR2[scFv]-PSIFs, (L) anti-VEGFR2[IgG]-NCSes. Values are shown as means ± SEM. $^{**}P < 0.01$; internalizing mAbs versus PBS by Bonferroni post hoc analysis with two-way ANOVA (n = 6).

human phage antibody libraries,[46,47] which have already been developed. This system can expand the versatility of phage display systems, which will thus contribute to the development of other cell-internalizing antibodies against various types of antigens for effective cancer therapy.

A comparison of cell-internalizing mAbs with low-internalizing mAbs revealed the strength of the cell-internalizing mAbs in terms of the biodistribution and therapeutic effects. Until now, how internalization contributes to the biodistribution of mAbs has been unclear. In this report, we could use a comparative study to clarify this question because we produced both cell-internalizing mAbs and low-internalizing mAbs with similar binding affinities. As a result, more cell-internalizing mAbs than low-internalizing mAbs were significantly accumulated in the tumor. This is the first evidence to support that mAbs with high internalization activity have greater tumor-targeting potency. This information is also useful for other applications that benefit from cell-internalizing mAbs, such as liposomal drugs, bioactive proteins/peptides, and viral vectors.[48,49]

Until now, the usefulness of Robo4-targeted therapy has not been established. Therapy to target VEGF-VEGFR signaling is already common, but the risk of side effects must be addressed.[31-33] Although VEGFR expression is upregulated on tumor vessels, it is also observed on the endothelium in healthy tissues. Previous reports also mentioned the toxicity associated with the anti-VEGFR therapies in mouse models[50] and the clinical trial.[51] Therefore, alternative therapies that target tumor angiogenesis are desired. In the present study, we revealed the possibility that anti-Robo4 ADCs were safer than anti-VEGFR2 ADCs, although they had similar antitumor effects. The findings from immunofluorescence and biodistribution studies also support the notion that anti-Robo4 mAbs could accumulate in the tumor without distributing to normal tissues. This is the first finding of Robo4-targeted therapy and suggests that Robo4 is a potential alternative target for tumor vascular targeting. Of course, additional experiments are needed to establish anti-Robo4 as a novel tool in tumor vascular targeting. For example, the pathological observations of normal blood vessels, in-depth toxicological analysis,

or the efficacy against other clinical relevant tumor models, are important for the successful story. Such basic analyses regarding Robo4 might accelerate the development of novel medicines that target tumor angiogenesis, including anti-Robo4 ADCs.

Acknowledgments

This study was supported by Grant-in-Aid for Scientific research (B) and Grant-in-Aid for Scientific Research on Innovative Areas from the Ministry of Education, Culture, Sports, Science, and Technology of Japan and the Japan Society for the Promotion of Science; Strategic Japanese-Swiss Cooperative Program from Japan Science and Technology Agency (JST) and the Swiss Federal Institute of Technology Zurich.

Authorship

Contribution: Y.M. designed the study; M.Y. and Y. Tsumori performed the experiments; Y.M. and M.Y. analyzed the data; Y.M. and M.Y. wrote the initial manuscript; S.T. and Y. Tsutsumi contributed to the phage display; Y.Y. and N.O. contributed to animal experiments; Y.O., W.C.A., and T.D. contributed to Robo4 related analysis; Y.M. and S.N. were responsible for the overall project. All authors edited the manuscript.

Conflict-of-interest disclosure: The authors declare no competing financial interests.

Correspondence: Yohei Mukai and Shinsaku Nakagawa, Laboratory of Biotechnology and Therapeutics, Graduate School of Pharmaceutical Sciences, Osaka University, 1–6 Yamadaoka, Suita, Osaka 565–0871, Japan; e-mail: y-mukai@nibio.go.jp and nakagawa@phs.osaka-u.ac.jp.

References

1. Alley SC, Okeley NM, Senter PD. Antibody-drug conjugates: targeted drug delivery for cancer. *Curr Opin Chem Biol.* 2010;14(4):529-537.
2. Isakoff SJ, Baselga J. Trastuzumab-DM1: building a chemotherapy-free road in the treatment of human epidermal growth factor receptor 2-positive breast cancer. *J Clin Oncol.* 2011;29(4): 351-354.
3. Ansell SM. Brentuximab vedotin: delivering an antimitotic drug to activated lymphoma cells. *Expert Opin Investig Drugs.* 2011;20(1):99-105.
4. Reichert JM. Antibody-based therapeutics to watch in 2011. *MAbs.* 2011;3(1):76-99.
5. Gerber HP, Senter PD, Grewal IS. Antibody drug-conjugates targeting the tumor vasculature: Current and future developments. *MAbs.* 2009; 1(3):247-253.
6. Poul MA, Becerril B, Nielsen UB, et al. Selection of tumor-specific internalizing human antibodies from phage libraries. *J Mol Biol.* 2000;301(5): 1149-1161.
7. An F, Drummond DC, Wilson S, et al. Targeted drug delivery to mesothelioma cells using functionally selected internalizing human single-chain antibodies. *Mol Cancer Ther.* 2008;7(3): 569-578.
8. Mukai Y, Sugita T, Yamato T, et al. Creation of novel Protein Transduction Domain (PTD) mutants by a phage display-based high-throughput screening system. *Biol Pharm Bull.* 2006;29(8):1570-1574.
9. Chaudhary VK, FitzGerald DJ, Adhya S, et al. Activity of a recombinant fusion protein between transforming growth factor type alpha and Pseudomonas toxin. *Proc Natl Acad Sci USA.* 1987;84(13):4538-4542.
10. Kreitman RJ, Wilson WH, Bergeron K, et al. Efficacy of the anti-CD22 recombinant immunotoxin BL22 in chemotherapy-resistant hairy-cell leukemia. *N Engl J Med.* 2001;345(4): 241-247.
11. Pastan I, FitzGerald D. Pseudomonas exotoxin: chimeric toxins. *J Biol Chem.* 1989;264(26): 15157-15160.
12. Legg JA, Herbert JMJ, Clissold P, et al. Slits and Roundabouts in cancer, tumour angiogenesis and endothelial cell migration. *Angiogenesis.* 2008; 11(1):13-21.
13. Huminiecki L, Bicknell R. In silico cloning of novel endothelial-specific genes. *Genome Res.* 2000; 10(11):1796-1806.
14. Huminiecki L, Gorn M, Suchting S, et al. Magic roundabout is a new member of the roundabout receptor family that is endothelial specific and expressed at sites of active angiogenesis. *Genomics.* 2002;79(4):547-552.
15. Smith-Berdan S, Nguyen A, Hassanein D, et al. Robo4 cooperates with CXCR4 to specify hematopoietic stem cell localization to bone marrow niches. *Cell Stem Cell.* 2011;8(1):72-83.
16. Park KW, Morrison CM, Sorensen LK, et al. Robo4 is a vascular-specific receptor that inhibits endothelial migration. *Dev Biol.* 2003;261(1): 251-267.
17. Seth P, Lin Y, Hanai J, et al. Magic roundabout, a tumor endothelial marker: expression and signaling. *Biochem Biophys Res Commun.* 2005; 332(2):533-541.
18. Okada Y, Yano K, Jin E, et al. A three-kilobase fragment of the human Robo4 promoter directs cell type-specific expression in endothelium. *Circ Res.* 2007;100(12):1712-1722.
19. Okada Y, Jin E, Nikolova-Krstevski V, et al. A GABP-binding element in the Robo4 promoter is necessary for endothelial expression in vivo. *Blood.* 2008;112(6):2336-2339.
20. Jones CA, London NR, Chen H, et al. Robo4 stabilizes the vascular network by inhibiting pathologic angiogenesis and endothelial hyperpermeability. *Nat Med.* 2008;14(4):448-453.
21. Jones CA, Nishiya N, London NR, et al. Slit2-Robo4 signalling promotes vascular stability by blocking Arf6 activity. *Nat Cell Biol.* 2009; 11(11):1325-1331.
22. Marlow R, Binnewies M, Sorensen LK, et al. Vascular Robo4 restricts proangiogenic VEGF signaling in breast. *Proc Natl Acad Sci USA.* 2010;107(23):10520-10525.
23. Koch AW, Mathivet T, Larrivée B, et al. Robo4 maintains vessel integrity and inhibits angiogenesis by interacting with UNC5B. *Dev Cell.* 2011;20(1):33-46.
24. Kerbel RS. Tumor angiogenesis. *N Engl J Med.* 2008;358(19):2039-2049.
25. Paleolog EM. Angiogenesis in rheumatoid arthritis. *Arthritis Res.* 2002;4(Suppl 3):S81-S90.
26. Tonnesen MG, Feng X, Clark RA. Angiogenesis in wound healing. *J Investig Dermatol Symp Proc.* 2000;5(1):40-46.
27. Olsson AK, Dimberg A, Kreuger J, et al. VEGF receptor signalling - in control of vascular function. *Nat Rev Mol Cell Biol.* 2006;7(5):359-371.
28. Crawford Y, Ferrara N. VEGF inhibition: insights from preclinical and clinical studies. *Cell Tissue Res.* 2009;335(1):261-269.
29. Wicki A, Rochlitz C, Orleth A, et al. Targeting tumor-associated endothelial cells: anti-VEGFR2 immunoliposomes mediate tumor vessel disruption and inhibit tumor growth. *Clin Cancer Res.* 2012;18(2):454-464.
30. Witmer AN, Dai J, Weich HA, et al. Expression of vascular endothelial growth factor receptors 1, 2, and 3 in quiescent endothelia. *J Histochem Cytochem.* 2002;50(6):767-777.
31. Kamba T, McDonald DM. Mechanisms of adverse effects of anti-VEGF therapy for cancer. *Br J Cancer.* 2007;96(12):1788-1795.
32. Eremina V, Jefferson JA, Kowalewska J, et al. VEGF inhibition and renal thrombotic microangiopathy. *N Engl J Med.* 2008;358(11):1129-1136.
33. Choueiri TK, Mayer EL, Je Y, et al. Congestive heart failure risk in patients with breast cancer treated with bevacizumab. *J Clin Oncol.* 2011; 29(6):632-638.
34. Yoshikawa M, Mukai Y, Okada Y, et al. Ligand-independent assembly of purified soluble magic roundabout (Robo4), a tumor-specific endothelial marker. *Protein Expr Purif.* 2008;61(1):78-82.
35. Imai S, Mukai Y, Nagano K, et al. Quality enhancement of the non-immune phage scFv library to isolate effective antibodies. *Biol Pharm Bull.* 2006;29(7):1325-1330.
36. Yoshikawa M, Mukai Y, Tsunoda S, et al. Modifying the antigen-immunization schedule improves the variety of monoclonal antibodies obtained from immune-phage antibody libraries against HIV-1 Nef and Vif. *J Biosci Bioeng.* 2011; 111(5):597-599.
37. Yamamoto Y, Tsutsumi Y, Yoshioka Y, et al. Site-specific PEGylation of a lysine-deficient TNF-alpha with full bioactivity. *Nat Biotechnol.* 2003;21(5):546-552.
38. Hunter WM, Greenwood FC. Preparation of iodine-131 labelled human growth hormone of high specific activity. *Nature.* 1962;194:495-496.
39. Mellman I. Endocytosis and molecular sorting. *Annu Rev Cell Dev Biol.* 1996;12:575-625.
40. Holliger P, Hudson PJ. Engineered antibody fragments and the rise of single domains. *Nat Biotechnol.* 2005;23(9):1126-1136.
41. Pavlinkova G, Beresford GW, Booth BJ, et al. Pharmacokinetics and biodistribution of engineered single-chain antibody constructs of MAb CC49 in colon carcinoma xenografts. *J Nucl Med.* 1999;40(9):1536-1546.
42. Schneider DW, Heitner T, Alicke B, et al. In vivo biodistribution, PET imaging, and tumor accumulation of 86Y- and 111In-antimindin/RG-1,

engineered antibody fragments in LNCaP tumor-bearing nude mice. *J Nucl Med.* 2009; 50(3):435-443.

43. Maeda H. SMANCS and polymer-conjugated macromolecular drugs: advantages in cancer chemotherapy. *Adv Drug Deliv Rev.* 2001;46(1-3): 169-185.
44. Kappen LS, Goldberg IH. Activation and inactivation of neocarzinostatin-induced cleavage of DNA. *Nucleic Acids Res.* 1978; 5(8):2959-2967.
45. Okamoto T, Mukai Y, Yoshioka Y, et al. Optimal construction of non-immune scFv phage display libraries from mouse bone marrow and spleen established to select specific scFvs efficiently binding to antigen. *Biochem Biophys Res Commun.* 2004;323(2): 583-591.
46. Silacci M, Brack S, Schirru G, et al. Design, construction, and characterization of a large synthetic human antibody phage display library. *Proteomics.* 2005;5(9): 2340-2350.
47. Villa A, Lovato V, Bujak E, et al. A novel synthetic naïve human antibody library allows the isolation of antibodies against a new epitope of oncofetal fibronectin. *MAbs.* 2011; 3(3):264-272.
48. Sapra P, Allen TM. Internalizing antibodies are necessary for improved therapeutic efficacy of antibody-targeted liposomal drugs. *Cancer Res.* 2002;62(24):7190-7194.
49. Pastan I, Hassan R, Fitzgerald DJ, et al. Immunotoxin therapy of cancer. *Nat Rev Cancer.* 2006;6(7):559-565.
50. Chinnasamy D, Yu Z, Theoret MR, et al. Gene therapy using genetically modified lymphocytes targeting VEGFR-2 inhibits the growth of vascularized syngenic tumors in mice. *J Clin Invest.* 2010;120(11):3953-3968.
51. Nagayama H, Matsumoto K, Isoo N, et al. Gastrointestinal bleeding during anti-angiogenic peptide vaccination in combination with gemcitabine for advanced pancreatic cancer. *Clin J Gastroenterol.* 2010;3(6):307-317.

—Foreword—

抗体工学による次世代バイオ創薬

角田慎一[a,b]

Antibody Engineering for Next-Generation Biodrug Development

Shin-ichi Tsunoda[a,b]

[a]*Laboratory of Biopharmaceutical Research, National Institute of Biomedical Innovation; 7-6-8 Saito-Asagi, Ibaraki, Osaka 567-0085, Japan: and* [b]*Laboratory of Biomedical Innovation, Graduate School of Pharmaceutical Sciences, Osaka University; 1-6 Yamadaoka, Suita, Osaka 565-0871, Japan.*

昨今のゲノム創薬研究，プロテオーム創薬研究の進展により，様々な疾患に関連する候補分子が同定され，それらの創薬標的としての可能性の検討が進められている．また，有望な標的分子に対しては，モノクローナル抗体製剤を始めとするバイオ医薬が次々と臨床に投入されており，がんや自己免疫疾患，感染症等の難治性疾患において，従来の低分子薬では達成できなかった顕著な治療効果を発揮している．このような抗体医薬開発の領域においては，新規な標的分子に対する治療薬の開発が試みられる一方で，先行薬と同じ標的分子に対しても，付加価値を加え高機能化した新薬，あるいは，改良型医薬である「バイオベター」の開発が積極的に進められている．また最近では，抗体医薬に抗がん剤を付加した antibody-drug conjugate（ADC）や，二重特異性抗体といった全くの人工的なフォーマットの抗体医薬も既に臨床で実用化されるに至っており，抗体医薬の開発が，今後益々進展することに疑う余地はない．

このように，抗体医薬の開発は現在，世界競争的に推進されているが，残念ながら，わが国の抗体医薬開発は欧米に大きく遅れをとっているのが現状である．ようやく近年，わが国の大手製薬メーカー各社も抗体医薬に力を注ぐようになり，わが国発の抗体医薬として，キャッスルマン病やリウマチ性疾患に対して抗 IL-6R 抗体（トシリズマブ）が，さらに最近になって，成人 T 細胞白血病リンパ腫に対して抗 CCR4 抗体（モガムリズマブ）が上市された．しかし，欧米の開発スピードに追いつき，追い越すためには，新たな創薬技術，すなわち，創薬標的分子の効率的な探索技術や，作製困難な分子に対する抗体の創製技術，高機能な抗体医薬の創製技術等の開発が不可欠であり，それらを産官学で力を合わせて推進することが必要と考えられる．

上記観点から，日本薬学会第 132 年会では，「抗体工学による次世代バイオ創薬」と題してシンポジウムを企画し，革新的抗体医薬の開発に資する研究について，基礎研究者や製薬メーカーの立場から紹介頂いた．本誌上シンポジウムでは，それらの研究を詳しく紹介して頂くために，ここに執筆をお願いした次第である．

鎌田春彦先生からは，創薬標的の効率的探索・絞り込み法としての「抗体プロテオミクス技術」についてご紹介頂いた．昨今のプロテオミクスのアプローチにより，疾患関連タンパク質の候補が多数同定されると，それらの中から，創薬標的として有望なタンパク質を効率よく絞り込むことが不可欠となる．その際には，各候補分子に対する抗体が不可欠なツールとなるが，タンパク質に対する抗体作製には，一般に多大な時間と労力を要する．したがって，抗体の作製がゲノム創薬・プロテオーム創薬における 1 つのボトルネックであり，この観点からも抗体の迅速作製技術が待望されている．抗体プロテオミクス技術は，上記ボトルネックを克服し，有望な創薬標的分子の絞り込みと，その後の開発を加速する技術として期待される．

加藤和則先生からは，薬剤運搬に適した腫瘍標的

[a]独立行政法人医薬基盤研究所バイオ創薬プロジェクト（〒567-0085 大阪府茨木市彩都あさぎ 7-6-8），[b]大阪大学大学院薬学研究科医薬基盤科学分野（〒565-0871 大阪府吹田市山田丘 1-6）
e-mail: tsunoda@nibio.go.jp

日本薬学会第 132 年会シンポジウム S08 序文

化抗体のスクリーニング法と創薬シーズ開発について紹介頂いた．抗体医薬開発においては，有用な標的分子の探索とともに，有望な抗体クローンの効率的なスクリーニング技術が必要となる．その点，加藤先生が開発されたProtein AのFc結合モチーフを発現するファイバー改変型アデノウイルスを利用した腫瘍特異的モノクローナル抗体のスクリーニング法は，ハイブリドーマライブラリの中から腫瘍標的化抗体を効率よく単離することが可能な技術である．今後，様々な抗体医薬や標的指向型DDS医薬等の開発に応用されるものと期待される．

八木秀樹先生からは，複数回膜貫通型膜タンパク質に対するモノクローナル抗体の効率的作製法についてご紹介頂いた．トランスポーターやGタンパク質共役受容体（G protein-coupled receptor; GPCR）は，細胞機能に重要な役割を果たす膜タンパク質である．2012年度のノーベル化学賞がGPCRの研究に授与されたことは，その機能的重要性を表しており，創薬標的としても有望である．しかし，複数回膜貫通型タンパク質は，脂溶性が高いことや，細胞外ドメインが小さいことなどの理由により，モノクローナル抗体の作製が困難であり，抗体医薬の開発にはいまだつながっていない．本観点から，八木先生らのグループでは，動物への免疫方法やスクリーニング法を工夫・最適化することにより，トランスポーターやGPCRの細胞外ドメインに対するモノクローナル抗体を効率よく作製し得る方法を確立した．本技術は，抗体医薬の標的分子の範囲拡大に貢献するものと期待される．

以上，本誌上シンポジウムの概要を紹介させて頂いた．各稿で紹介されている次世代バイオ創薬の技術やコンセプトが，近い将来，わが国発の革新的医薬品や疾患治療法を生み出す一助となることを願っている．

Cytokine 61 (2013) 578–584

Contents lists available at SciVerse ScienceDirect

Cytokine

journal homepage: www.journals.elsevier.com/cytokine

Mutants of lymphotoxin-α with augmented cytotoxic activity *via* TNFR1 for use in cancer therapy

Tomohiro Morishige [a,1], Yasuo Yoshioka [b,c,*,1], Shogo Narimatsu [a], Shinji Ikemizu [d], Shin-ichi Tsunoda [c,e], Yasuo Tsutsumi [b,c,e], Yohei Mukai [a], Naoki Okada [a], Shinsaku Nakagawa [a,c,*]

[a] *Laboratory of Biotechnology and Therapeutics, Graduate School of Pharmaceutical Sciences, Osaka University, 1-6 Yamadaoka, Suita, Osaka 565-0871, Japan*
[b] *Laboratory of Toxicology and Safety Science, Graduate School of Pharmaceutical Sciences, Osaka University, 1-6 Yamadaoka, Suita, Osaka 565-0871, Japan*
[c] *The Center for Advanced Medical Engineering and Informatics, Osaka University, 1-6 Yamadaoka, Suita, Osaka 565-0871, Japan*
[d] *Graduate School of Pharmaceutical Sciences, Kumamoto University, 5-1 Oe-honmachi, Kumamoto 862-0973, Japan*
[e] *Laboratory of Biopharmaceutical Research, National Institute of Biomedical Innovation, 7-6-8 Saito-Asagi, Ibaraki, Osaka 567-0085, Japan*

ARTICLE INFO

Article history:
Received 6 July 2012
Received in revised form 29 September 2012
Accepted 6 November 2012
Available online 11 December 2012

Keywords:
Affinity
Apoptosis
Bioactivity
Cytokine
Cytotoxicity

ABSTRACT

The cytokine lymphotoxin-α (LTα) is a promising candidate for use in cancer therapy. However, the instability of LTα *in vivo* and the insufficient levels of tumor necrosis factor receptor 1 (TNFR1)-mediated bioactivity of LTα limit its therapeutic potential. Here, we created LTα mutants with increased TNFR1-mediated bioactivity by using a phage display technique. We constructed a phage library displaying lysine-deficient structural variants of LTα with randomized amino acid residues. After affinity panning, we screened three clones of lysine-deficient LTα mutant, and identified a LTα mutant with TNFR1-mediated bioactivity that was 32 times that of the wild-type LTα (wtLTα). When compared with wtLTα, the selected clone showed augmented affinity to TNFR1 due to slow dissociation rather than rapid association. In contrast, the mutant showed only 4 times the TNFR2-mediated activity of wtLTα. In addition, the LTα mutant strongly and rapidly activated caspases that induce TNFR1-mediated cell death, whereas the mutant and wtLTα activated nuclear factor-kappa B to a similar extent. Our data suggest that the kinetics of LTα binding to TNFR1 play an important role in signal transduction patterns, and a TNFR1-selective LTα mutant with augmented bioactivity would be a superior candidate for cancer therapy.

1. Introduction

Lymphotoxin-alpha (LTα) is a tumor necrosis factor (TNF) superfamily cytokine with tumor-cell-specific cytotoxic activity and immune-activating activity. LTα induces the expression of chemokines and adhesion molecules in endothelial cells, and plays a key role in lymph node neogenesis [1–3]. Schrama et al. [4,5] showed that systemic administration of LTα to a tumor-bearing mouse leads to the construction of ectopic lymphoid tissue within the tumor and the strong induction of tumor immunity in that lymphoid tissue, suggesting that the underlying mechanism of this cytokine's anti-tumor activity may be effective. Therefore, LTα has long been considered to be a promising candidate for an anti-cancer agent. However, the clinical use of LTα has been limited because of the protein's *in vivo* instability and proinflammatory side effects.

One of the most common ways to improve the therapeutic effects of proteins is to conjugate them with polyethylene glycol (PEG) in a process called PEGylation, or to conjugate them with other water-soluble polymers [6]. Because of the steric hindrance caused by the PEG molecule, PEGylation can prolong the plasma half-life of molecules and alter the tissue distribution of the conjugates compared with those of the native form. PEGylation of proteins is mostly nonspecific because it targets all of the lysine residues in the protein, some of which may be in or near an active site. As a result, PEGylation significantly reduces the specific

Abbreviations: E. coli, Escherichia coli; ELISA, enzyme-linked immunosorbent assay; FADD, Fas-associated protein with death domain; FBS, fetal bovine serum; HVEM, herpes virus entry mediator; IFNγ, interferon γ; LTα, lymphotoxin-alpha; NFκB, nuclear factor-kappa B; PEG, polyethylene glycol; pI, isoelectric points; SDS–PAGE, sodium dodecyl sulfate–polyacrylamidegel electrophoresis; SPR, surface plasmon resonance; TNF, tumor necrosis factor; TNFR1, TNF receptor 1; TRADD, TNF receptor-associated death domain; TRAF, TNF receptor-associated factor; wtLTα, wild-type LTα.

* Corresponding authors. Addresses: Laboratory of Toxicology and Safety Science, Graduate School of Pharmaceutical Sciences, Osaka University, 1-6 Yamadaoka, Suita, Osaka 565-0871, Japan. Tel./fax: +81 6 6879 8233 (Y. Yoshioka), Laboratory of Biotechnology and Therapeutics, Graduate School of Pharmaceutical Sciences, Osaka University, 1-6 Yamadaoka, Suita, Osaka 565-0871, Japan. Tel.: +81 6 6879 8175; fax: +81 6 6879 8179 (S. Nakagawa).

E-mail addresses: yasuo@phs.osaka-u.ac.jp (Y. Yoshiokab), nakagawa@phs.osaka-u.ac.jp (S. Nakagawa).

[1] These authors contributed equally to the work.

1043-4666/$ - see front matter © 2012 Elsevier Ltd. All rights reserved.
http://dx.doi.org/10.1016/j.cyto.2012.11.005

activity of the proteins involved. Our group previously developed a novel strategy for site-specific mono-PEGylation of lysine-deficient mutants to overcome these limitations of PEGylation [7,8]. We demonstrated that site-specific PEGylation of a lysine-deficient mutant of LTα retained higher bioactivity compared with random PEGylation of wild-type LTα (wtLTα) [9]. This finding suggests that site-specific PEGylation of a lysine-deficient mutant of LTα might be a useful way to overcome the problems in the clinical use of LTα outlined above.

LTα binds to three receptor subtypes—TNF receptor 1 (TNFR1), TNFR2, and herpes virus entry mediator (HVEM)—to exert various biological functions. TNFR1 induces an anti-tumor effect and Peyer's patch development, whereas TNFR2 is essential for immune responses against bacteria and viruses [1]. Human LTα and TNF that bind to murine TNFR1, but not to murine TNFR2, are not lethal in healthy mice except at extremely high doses, suggesting that LTα and TNF α exhibit their lethal side effects *via* TNFR2 [10,11]. Therefore, LTα as a cancer immunotherapeutic agent, a LTα mutant with selectively increased TNFR1-mediated bioactivity is needed. Previously, we successfully created a TNFR1-selective LTα mutant whose bioactivity *via* TNFR1 was several times that of wtLTα, and whose bioactivity *via* TNFR2 was 2.5% that of wtLTα [12]. However, to enhance therapeutic efficacy and suppress the side effect of LTα, it is necessary to create a LTα mutant with greatly increased TNFR1-mediated bioactivity and TNFR1-selectivity.

In this study, we attempted to create LTα mutants with selectively increased TNFR1-mediated bioactivity by using a phage display technique. We succeeded in creating a LTα mutant that had a much higher bioactivity *via* TNFR1 and an augmented affinity to TNFR1 compared with that of wtLTα, and demonstrated that this was due to the slow dissociation rate of the LTα mutant-TNFR1 complex. In addition, we showed that the LTα mutant differed from wtLTα by its ability to strongly and rapidly activate caspases. In contrast, the LTα mutant and wtLTα were similar to each other in their degree of activation of nuclear factor-kappa B (NFκB). Our findings suggest that this LTα mutant would be a superior candidate for a cancer immunotherapeutic agent.

2. Materials and methods

2.1. Cells

HEp-2 cells, a human carcinoma cell line derived via HeLa contamination, were purchased from the American Type Culture Collection (Manassas, VA), and cultured in RPMI 1640 medium (Wako Pure Chemical Industries, Osaka, Japan) supplemented with 10% fetal bovine serum (FBS), 1 mM sodium pyruvate, 50 μM 2-mercaptoethanol, and antibiotics. HT29.14S cells, a TNF/LT-sensitive subclone of HT29 human colon adenocarcinoma, were kindly provided by Dr. Carl Ware (La Jolla Institute for Allergy and Immunology, CA) [13]. HT29.14S cells were cultured in Dulbecco's Modified Eagle's Medium (Wako Pure Chemical Industries) supplemented with 10% FBS, 10 mM HEPES, and antibiotics. hTNFR2/mFas-PA cells are preadipocytes derived from TNFR1$^{-/-}$ TNFR2$^{-/-}$ mice expressing a chimeric receptor composed of the extracellular and transmembrane domain of human TNFR2 and the intracellular domain of mouse Fas, which is a member of the TNF receptor superfamily [14]; these cells were cultured in RPMI 1640 medium supplemented with 10% FBS, 5 μg/mL Blasticidin S HCl (Invitrogen, Carlsbad, CA), and antibiotics. MCF-7 cells were provided from the Institute of Development, Aging and Cancer, Tohoku University, and were cultured in Eagle's Minimum Essential Medium (Wako Pure Chemical Industries) supplemented with 10% FBS, 0.01 mg/mL bovine insulin, and antibiotics.

2.2. Construction of a library of lysine-deficient mutants of LTα

The phagemid vector pY03′, which encodes human wtLTα with the C-terminus of wtLTα fused to the N-terminus of the M13 phage g3p, was used as a PCR template for constructing a DNA library of lysine-deficient mutants of LTα. We performed a two-step PCR amplification using oligonucleotides containing the sequence NNS (where N represents A, C, G, or T; and S represents C or G) at Lys19, Lys28, Lys39, Lys84, Lys89, and Lys119 of wtLTα; the sequence NNS encodes all 20 standard amino acids. The products from the second PCR were digested with *Nco*I and *Pst*I and then ligated into pY03′. The phagemid was electroporated into *Escherichia coli* (*E. coli*) TG1 cells (Stratagene, Cedar Creek, TX), yielding 2×10^6 independent clones. The phage library displaying lysine-deficient LTα molecules was prepared as described previously [12]. Briefly, pY03′-transformed TG1 cells were infected with M13KO7 helper phage (Invitrogen) and cultured for 6 h at 25 °C. The resultant phage particles were precipitated from the culture supernatant by using PEG (MP Biomedicals, Solon, OH) and suspended in NTE (100 mM NaCl, 10 mM Tris, 1 mM EDTA).

2.3. Selection of bioactive LTα mutants

Screening for bioactive LTα mutants was performed as described previously [12]. Briefly, an immunoplate was coated with soluble human TNFR1 (R&D Systems, Minneapolis, MN), and the prepared phage library was allowed to bind to the immobilized TNFR1. After a second round of panning, single colonies were picked and cultured. The resulting phage-containing culture supernatant was used for screening by enzyme-linked immunosorbent assay (ELISA) against human TNFR1.

2.4. Expression and purification of recombinant LTαs

pET15b plasmids (Novagen, Darmstadt, Germany) encoding LTαs were prepared and used to transform *E. coli* BL21(DE3) cells (Stratagene) for the expression of recombinant protein, as described previously [12]. Expression was induced by adding 1 mM isopropyl β-D-1-thiogalactopyranoside and incubating the cells at 37 °C for 6 h in Terrific Broth (Invitrogen Corporation, Carlsbad, CA) containing 0.4% glucose, 1.68 mM $MgSO_4$, and 100 μg/mL of ampicillin; all products were accumulated as inclusion bodies. The resultant inclusion bodies were washed, solubilized, reduced, and refolded by the methods previously described [12]. After dialysis against a buffer containing 20 mM Tris–HCl (pH 7.4) and 100 mM urea, active trimeric LTα proteins were purified by using a HiLoad Superdex 200PG column (GE Healthcare, UK) equilibrated with phosphate-buffered saline (pH 7.4) followed by ion-exchange chromatography (SP Sepharose Fast Flow for wtLTα; Q Sepharose Fast Flow for mutants of LTα); both columns were obtained from GE Healthcare. To create point mutants, we used pET15b-human wtLTα as a template with a KOD-plus mutagenesis kit (Toyobo, Osaka, Japan) according to the manufacturer's instructions. Recombinant point mutants were produced and purified as described earlier; SP Sepharose Fast Flow was used as the ion-exchange column. Protein concentration was measured by using Coomassie Protein Assay Reagent (Thermo Fisher Scientific, Rockford, IL). Sodium dodecyl sulfate–polyacrylamidegel electrophoresis (SDS–PAGE) analysis of LTαs was conducted under reducing conditions, and the proteins in the gels were stained with Coomassie brilliant blue. The electrostatic potential surface was generated by using GRASP software [15]. The electrostatic potential ranged from −7.5 kT to 7.5 kT. The relative accessible surface areas were calculated by using JOY software [16].

2.5. Cytotoxicity assays

HEp-2 cells were seeded at 4×10^4 cells per well in 96-well plates and incubated for 18 h with serially-diluted LTαs in the presence of 50 μg/mL cycloheximide. For the functional blocking assay, HEp-2 cells were treated with serially-diluted MAB225 (R&D Systems), an anti-TNFR1 antibody, for 30 min. The cells were then incubated with 100 ng/mL wtLTα and LTα mutants for 18 h in the presence of 50 μg/mL cycloheximide. For the caspase inhibition assay, HEp-2 cells were incubated with serially-diluted wtLTα or LTα mutants in the presence of 50 μg/mL cycloheximide and 50 mM zVAD-fmk (Calbiochem, Darmstadt, Germany) for 18 h. R2/Fas preadipocyte cells were seeded at 1.5×10^4 cells per well in 96-well plates and incubated for 48 h with serially-diluted LTαs in the presence of 50 μg/mL cycloheximide. The cytotoxicities of LTαs against HEp-2 cells and R2/Fas preadipocyte cells were assessed by using the standard methylene blue assay method as previously described [12]. HT29.14S and MCF-7 cells were seeded at 5×10^3 cells per well and incubated with LTαs in the presence of 80 U/mL human Interferon γ (IFNγ) (R&D Systems) for 72 h. After incubation, cell viability was measured by using a WST-8 assay kit (Nacalai Tesque, Kyoto, Japan) according to the manufacturer's instructions. The ratio of TNFR1-/TNFR2-mediated bioactivity was calculated as follows: activity of LTαs in HEp-2 cells/activity of LTαs in R2/Fas preadipocyte cells. The TNFR1/TNFR2 ratio for wtLTα was set equal to 1.

2.6. Analysis of binding kinetics by surface plasmon resonance

The binding kinetics of LTαs were analyzed and compared by using a surface plasmon resonance (SPR) method (BIAcore 2000, GE Healthcare, UK). Human TNFR1, TNFR2, or HVEM Fc chimera (R&D Systems, Inc.) was diluted to 50 μg/mL in 10 mM sodium acetate (pH 4.5) and immobilized onto a CM5 sensor chip by using an amine coupling kit (GE Healthcare, UK) as described previously [12]. During the association phase, wtLTα or LTα mutants diluted in HBS-EP running buffer (GE, Healthcare UK) to 37, 18.5, 9.3, 4.6, or 2.3 nM were passed over the immobilized TNFRs for 2 min at a flow rate 20 μL/min. During the dissociation phase, HBS-EP was run over the sensor chip for 1 min at a flow rate 20 μ L/min. Complexes were eluted by using 20 μL of 10 mM glycine–HCl (pH 2.0). Data were evaluated by using BIAevaluation 4.1 software (GE Healthcare UK) to apply a 1:1 Langmuir binding model. The obtained sensorgrams were fitted globally over the range of injected concentrations and simultaneously over the association and dissociation phases.

2.7. Evaluation of caspase-3/7 and -8 activities

HEp-2 cells were seeded at 4×10^4 cells per well in 96-well plates and then incubated for 6, 12, or 18 h with 10 ng/mL of the relevant LTα in the presence of 50 μg/mL cycloheximide. Activities of intracellular caspase-8 and caspase-3/7 were measured by using Caspase-Glo assays (Promega, Madison, WI) according to the manufacturer's instructions.

2.8. Evaluation of NFκB activities

HEp-2 cells were co-transfected with pGL4.32, a NFκB-responsive firefly luciferase expression vector, and pRL-TK, a thymidine kinase–regulated renilla luciferase expression vector (Promega) at a ratio of 90:1 for 18 h. The cells were then treated with 10 ng/mL of wtLTα or LTα mutants for 1, 2, 4, 6, 12, and 24 h. Expression levels of intracellular firefly luciferase and renilla luciferase were then measured by using the Dual-Luciferase Reporter Assay System (Promega). The expression level of firefly luciferase was normalized against that of renilla luciferase.

3. Results

3.1. Production of a highly bioactive LTα mutant

Our recent study showed that site-specific PEGylation of a lysine-deficient mutant of LTα might be useful for cancer therapy, because the mutant retained bioactivity after PEGylation [9]. Here, we attempted to create a lysine-deficient mutant of LTα with augmented bioactivity *via* TNFR1 and TNFR1-selective bioactivity that could be used for site-specific PEGylation in the future. A phage library displaying LTα mutants with randomized sequences in place of all lysine codons was prepared. For the construction of the phage library, two-step PCR was used to replace the lysine codons randomly with an NNS sequence. As a result, we successfully constructed a library with 2×10^6 independent clones, and performed two rounds of panning against immobilized human TNFR1; phage clones were screened for binding affinity to TNFR1 by conducting an ELISA (data not shown). We obtained three LTα mutants (mutLT1, mutLT2, and mutLT3), which were putative lysine-deficient mutants of LTα. DNA sequencing analysis of the LTα mutants confirmed that all 6 lysine residues present in wtLTα were mutated to other amino acids (Table 1). To investigate the properties of the LTα mutants in detail, we prepared recombinant LTα mutant proteins by using an *E. coli* expression system, as previously described [12]. LTα mutants and wtLTα were expressed in *E. coli* and obtained through refolding of inclusion bodies. Purified LTα mutants displayed a molecular mass of 18 kDa by SDS–PAGE analysis (Fig. 1A), and a molecular mass of approximately 60 kDa by size exclusion chromatography (Fig. 1B), indicating that LTα mutants form homotrimeric complexes, as does wtLTα. The isoelectric points (pI) of mutLT1, mutLT2, and mutLT3 were 6.16, 6.16, and 6.00, respectively whereas that of wtLTα was 8.94 (Table 1). We also visually assessed the changes in the surface electrostatic potential values by using GRASP software (Fig. 1C). Because of their lack of lysine residues, LTα mutants had more negative areas on their surface than did wtLTα.

3.2. Bioactivities of LTα mutants

To assess the TNFR1-mediated bioactivity of LTα mutants, cytotoxicity assays using HEp-2 cells were performed (Fig. 2A). wtLTα and LTα mutants showed dose-dependent cytotoxicity, and the bioactivity of each LTα mutant was higher than that of wtLTα in the HEp-2 cells (Fig. 2A). The bioactivity of mutLT1 was especially high (31.8 times that of wtLTα; Table 2). Furthermore, we confirmed that the LTα-induced cytotoxicity was blocked by the anti-TNFR1 antibody in all cases (Fig. 2B). These results indicate that the LTα mutants possess higher TNFR1-mediated bioactivity than that displayed by wtLTα. To confirm that the higher bioactivity of the LTα mutants was not specific to HEp-2 cells, we examined the bio-

Table 1
Amino acid sequences and the isoelectric points of LTα mutants. The pI values of LTαs were calculated by using a program in the Expert Protein Analysis System proteomics server of the Swiss Institute of Bioinformatics (Basel, Switzerland).

	Residue position						pI
	19	28	39	84	89	119	
wtLTα	Lys	Lys	Lys	Lys	Lys	Lys	8.94
mutLT1	Asn	Gln	Asn	Ser	Leu	Gly	6.16
mutLT2	Asn	Gln	Ser	Thr	Val	Val	6.16
mutLT3	Asp	Gln	Ala	Thr	Thr	Ala	6.00

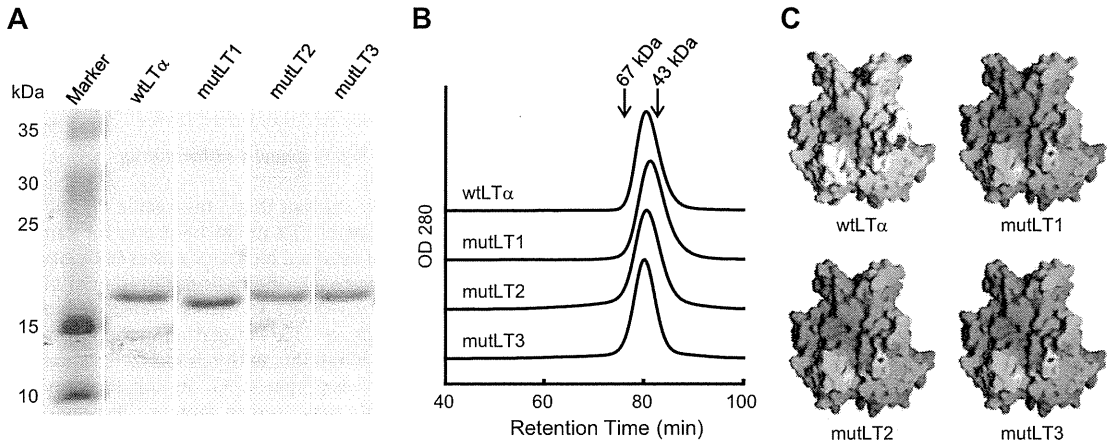

Fig. 1. Properties of recombinant LTα mutants. (A) SDS–PAGE analysis of wtLTα and LTα mutants. All products were separated on an SDS–PAGE gel and visualized by means of Coomassie Brilliant Blue staining. Marker indicates molecular weight standards. (B) Chromatograms of purified wtLTα and LTα mutants. wtLTα or LTα mutants were loaded onto a size-exclusion column and eluted at 1.0 mL/min. (C) The electrostatic potential surface was generated by using GRASP software. Red and blue indicate negative and positive electrostatic potentials, respectively. The electrostatic potential ranged from −7.5 kT (bright blue) to 7.5 kT (bright red). The relative accessible surface areas were calculated by using JOY software.

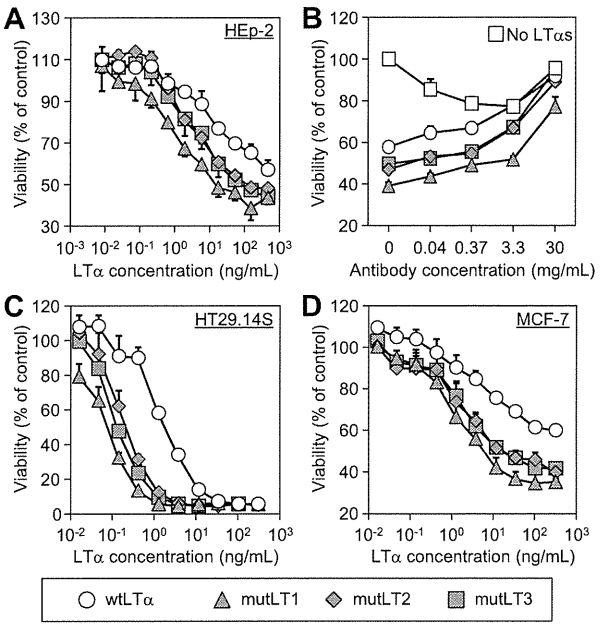

Fig. 2. TNFR1-mediated cytotoxic activity of wtLTα and LTα mutants. (A) HEp-2 cells were incubated with wtLTα or LTα mutants in the presence of cycloheximide. After 18 h incubation, cell viability was assessed by methylene blue assay. (B) HEp-2 cells were treated with serially-diluted MAB225, an anti-TNFR1 neutralizing antibody, for 30 min. The cells were then incubated with 100 ng/mL wtLTα or LTα mutants in the presence of cycloheximide. After 18 h incubation, the cell viability was assessed by methylene blue assay. (C) HT29.14S cells and (D) MCF-7 cells were incubated with wtLTα or LTα mutants in the presence of IFNγ. After 72 h incubation, the cell viability was assessed by WST-8 assay. EC30 and EC50 are the concentrations of LTα required for 30% and 50% inhibition of cell viability, respectively. Each value represents the mean ± SD ($n = 4$).

activities of mutLTαs in two other cell types (Fig. 2C and D, Table 2). When compared with wtLTα, the LTα mutants exhibited 8–24 times the cytotoxicity in HT29.14S cells, and 16–34 times the cytotoxicity in MCF-7 cells (Fig. 2C and D, Table 2). To specifically evaluate the TNFR2-mediated bioactivity of the LTα mutants, we examined the levels of cytotoxity induced by LTα mutants in hTNFR2/mFas-PA cells. These cells have been engineered to exhibit hTNFR2- but not hTNFR1-mediated activities [14]. The human TNFR2-mediated bioactivities of LTα mutants were 2.2–4.1 times those of wtLTα in hTNFR2/mFas-PA cells (Fig. 3). The calculated ratios of TNFR1-mediated bioactivity by using HEp-2 cells/TNFR2-mediated bioactivity induced by mutLT1, mutLT2, and mutLT3 were 7.8, 3.2, and 1.9 times that of wtLTα, respectively. This result suggests that LTα mutants, especially mutLT1, have selectivity for TNFR1 in addition to their augmented bioactivity.

Next, to measure the binding affinity of LTα mutants to TNFRs, we performed an SPR analysis by using a BIAcore 2000 biosensor (Table 3). The binding affinities of mutLT1, mutLT2 and mutLT3 to TNFR1 were 2.7, 2.0, and 1.4 times those of wtLTα, respectively. We considered that the increased affinity of LTα mutant for TNFR1 might be related to the enhanced bioactivity through this receptor. In particular, k_{off} values for LTα mutants binding to TNFR1 were 39–57% of the value for wtLTα, whereas the k_{on} values for LTα mutants binding to TNFR1 were almost the same as that for wtLTα. These results suggest that TNFR1 interacts more strongly with the LTα mutants than wtLTα due to slow dissociation kinetics, and that this binding mode between LTα mutant and TNFR1 induces a potent signaling pathway. We then evaluated the affinity of the LTα mutants for TNFR2 by using SPR methodology (Table 4). The affinity of TNFR2 for LTα mutants was 1.5–2.1 times that for wtLTα due to fast association kinetics. Taken together, these results indicate that the binding modes of LTα mutants to TNFR1 and TNFR2 might dictate their bioactivity.

We previously demonstrated that Lys84 in LTα plays a crucial role in the protein's interaction with the main chain of TNFR1 [12]. Therefore, to investigate the importance of the amino acid sequence at position 84, we created LTα mutants with Lys84 replaced by Ser84 (K84S), Thr84 (K84T), or Ala84 (K84A), and evaluated their binding kinetics and bioactivities *via* TNFR1. We found that these point mutants exhibited a slower dissociation rate and increased bioactivity *via* TNFR1 when compared with wtLTα. K84S showed especially high bioactivity even though its affinity for TNFR1 was lower than that of wtLTα (Table 5).

3.3. Activation of caspases by LTα mutant

It is known that TNFR1-mediated cell death is regulated by the activities of caspases including caspase-3, -7, and -8 [17].

Table 2
The TNFR1-mediated bioactivities of wtLTα and LTα mutants. EC30 and EC50 were calculated from the cytotoxic activity of wtLTα and LTα mutants against HEp-2, HT29.14S and MCF-7 cells. Relative activity values were calculated as EC30 (wtLTα)/EC30 (LTα mutant) or EC50 (wtLTα)/EC50 (LTα mutant).

	HEp-2 cells		HT29.14S cells		MCF-7 cells	
	EC30 (ng/mL)	Relative activity	EC50 (ng/mL)	Relative activity	EC50 (ng/mL)	Relative activity
wtLTα	47.7	1.0	1.80	1.0	36.7	1.0
mutLT1	1.5	31.8	0.08	23.6	1.1	33.7
mutLT2	6.8	7.0	0.21	8.5	2.3	16.0
mutLT3	7.8	6.1	0.13	14.2	2.3	16.0

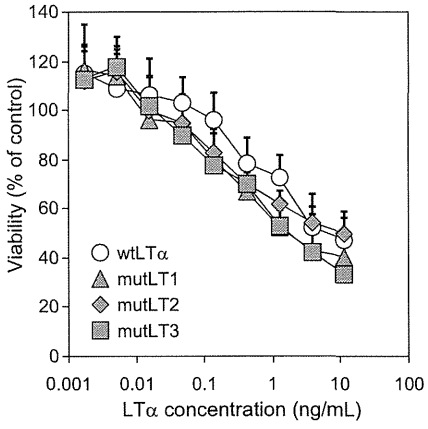

	EC30 (ng/mL)	Relative activity (% vs wtLTα)
wtLTα	1.39	100
mutLT1	0.34	409
mutLT2	0.64	217
mutLT3	0.43	323

Fig. 3. TNFR2-mediated cytotoxic activities of wtLTα and LTα mutants. hTNFR2/mFas-PA cells were incubated with serial dilutions of wtLTα or LTα mutants in the presence of cycloheximide. After 48 h incubation, cell viability was assessed by methylene blue assay. EC30 is the concentration of LTα required for 30% inhibition of cell viability. Each value represents the mean ± SD ($n = 4$).

Table 3
The binding kinetics of interactions between LTα mutants and hTNFR1 analyzed by using an SPR biosensor. k_{on} is the association kinetic constant; k_{off} is the dissociation kinetic constant; and K_D is the equilibrium dissociation constant. Relative affinity values were calculated as 100 × K_D (wtLTα)/K_D (LTα mutant).

	k_{on} (10^6/M s)	k_{off} (10^{-4}/s)	K_D (10^{-10}/M)	Relative affinity (% vs wtLTα)
wtLTα	1.2	6.1	4.9	100
mutLT1	1.3	2.4	1.8	269
mutLT2	1.4	3.5	2.5	195
mutLT3	0.97	3.4	3.4	143

Therefore, to examine the mechanism behind the augmentation of TNFR1-mediated bioactivity, we investigated the association between caspase activity and LTα mutant-induced cell death. First, we treated cells with LTα mutants in the presence of a broad caspase inhibitor, zVAD-fmk, and analyzed the cell viability (Fig. 4A). The results showed that zVAD-fmk almost completely abrogated the cytotoxicity induced by wtLTα and LTα mutants. These results indicate that both wild-type and LTα mutant-induced cell death were dependent on the activation of caspase. We then examined the activity of caspase-3/7 (Fig. 4B) and -8 (Fig. 4C) induced by LTα mutants in HEp-2 cells. LTα mutants, especially

Table 4
Binding kinetics of interactions between LTα mutants and hTNFR2 were analyzed by using an SPR biosensor. k_{on} is the association kinetic constant; k_{off} is the dissociation kinetic constant; and K_D is the equilibrium dissociation constant. Relative affinity values were calculated as 100 × K_D (wtLTα)/K_D (LTα mutant).

	k_{on} (10^6/M s)	k_{off} (10^{-4}/s)	K_D (10^{-10}/M)	Relative affinity (% vs wtLTα)
wtLTα	2.8	23.5	8.3	100
mutLT1	4.7	25.0	5.4	154
mutLT2	6.2	24.0	3.9	213
mutLT3	4.5	25.3	5.6	148

mutLT1, which has the highest bioactivity, quickly and strongly induced the activation of caspases. These results suggest that stabilization of the LTα -TNFR1 complex by the presence of LTα mutant contributed to increased caspase activity, which in turn induced cytotoxic effects.

3.4. Activation of NFκB by LTα mutants

It is well known that TNFR1 activates NFκB signaling pathway in addition to the caspase cascade [18,19]. Therefore, to investigate whether the LTα mutants activate NFκB, we assessed the association between NFκB activity and LTα mutant-induced cell death. First, we prepared cells transfected with luciferase expressing vector activated by NFκB. Then, we treated cells with LTα mutants and analyzed the NFκB activity by measuring the expression level of luciferase (Fig. 5). Despite the higher TNFR1-mediated bioactivity of LTα mutants, we found that NFκB activity was induced to a similar extent by LTα mutants and wtLTα. This finding indicates that the LTα mutants selectively activate the caspase cascade but not NFκB activation *via* TNFR1.

4. Discussion

When constructing a LTα mutant as an anti-cancer agent, it is important that the mutant exhibits TNFR1 selectivity because of the lethal side-effects of TNFR2-mediated bioactivity. We previously created a LTα mutant (R1selLT), which had only 2.5% of the TNFR2-mediated bioactivity of wtLTα and 3.5 times of the TNFR1-mediated bioactivity of wtLTα [12]. The ratio of TNFR1/TNFR2 bioactivity of R1selLT was 145.8 times that of wtLTα. In addition to TNFR1 selectivity, augmentation of TNFR1-mediated bioactivity is also highly desirable in a therapeutic agent for cancer. Here, we created three lysine-deficient LTα mutants with greatly increased levels of TNFR1-mediated bioactivity through an altered binding mode. These mutants showed preferentially augmented bioactivity *via* TNFR1 compared with TNFR2. The TNFR1 selectivity of mutLT1, 2, and 3 was 7.8, 3.2, and 1.9 times that of wtLTα, respectively. Although the TNFR1 selectivity was lower for mutLT1 than for R1selLT, the TNFR1-mediated bioactivity of mutLT1 was 31.8 times that of wtLTα compared to 3.5 times of R1selLT. Such extreme augmentation of bioactivity is rarely reported. As

Table 5
Binding kinetics of interactions between point-mutated LTαs and hTNFR1 were analyzed by using an SPR biosensor. k_{on} is the association kinetic constant; k_{off} is the dissociation kinetic constant; and K_D is the equilibrium dissociation constant. Relative affinity values were calculated as 100 × K_D (wtLTα)/K_D (point mutated LTα). TNFR1-mediated relative activities of LTα mutants were calculated from the concentration of LTα required for 30% inhibition of HEp-2 cell viability.

	k_{on} (10^6/M s)	k_{off} (10^{-4}/s)	K_D (10^{-10}/M)	Relative affinity (% vs wtLTα)	Relative activity(% vs wtLTα)
wtLTα	1.2	6.1	4.9	100	100
K84S	0.28	2.2	8.0	62	4810
K84T	1.0	4.3	118	195	1100
K84A	1.5	5.3	3.5	143	910

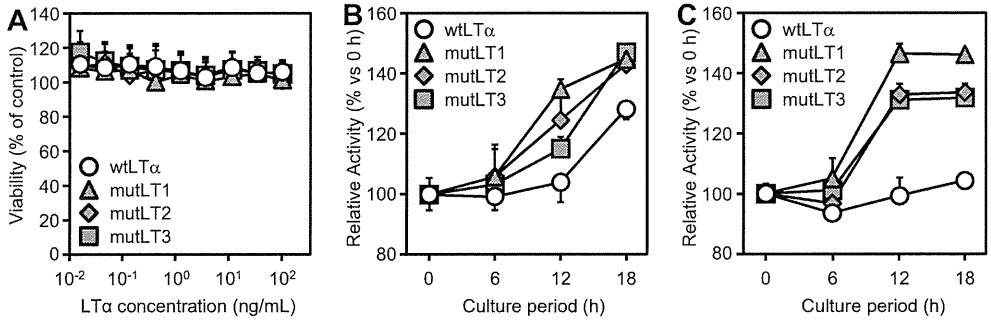

Fig. 4. Caspase activities in HEp-2 cells treated with wtLTα or LTα mutants. (A) Cycloheximide treated HEp-2 cells were incubated with wtLTα or LTα mutants in the presence of zVAD-fmk. After 18 h incubation, cell viability was assessed by methylene blue assay. (B and C) Cycloheximide treated HEp-2 cells were incubated for 6, 12, or 18 h with 10 ng/mL LTαs, and the activities of intracellular caspase-3/7 (B) and intracellular caspase-8 (C) were measured by using Caspase-Glo assays. Each value represents the mean ± SD (n = 4).

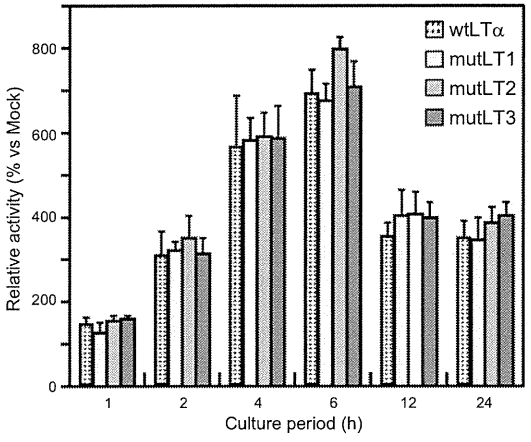

Fig. 5. NFκB activities in HEp-2 cells treated with wtLTα or LTα mutants. HEp-2 cells were co-transfected with pGL4.32 and pRL-TK (Promega). Eighteen hours after transfection, the cells were treated with 10 ng/mL LTαs for the indicated period. The intracellular luciferase activity was then quantified. Data are shown as the relative NFκB activity compared with the mock-transfected group. Each bar represents the mean ± SD (n = 4).

described above, high TNFR1 selectivity of R1selLT was mainly resulted from the significant decreased TNFR2-mediated bioactivity. On the other hand, the TNFR1 selectivity of mutLT1 was obtained from the augmented TNFR1-mediated bioactivity, while TNFR2-mediated bioactivity was maintained. On this point, TNFR2 is known to play essential role for the induction of immune responses. Therefore, we consider that a TNFR1-selective LTα mutants with high TNFR1-mediated and equivalent TNFR2-mediated bioactivity compared to wtLTα, such as mutLT1, would be a superior candidate for cancer therapy by combination of direct pro-apoptotic effects of LTα on tumor cells and an enhancement of local/systemic immunity.

Many cellular signaling processes are hypothesized to depend not only on the equilibrium strength of the ligand–receptor interactions but also on the average durations or kinetic dissociation rates of these interactions [20–23]. In some cases, the intensity of distal signaling depends on the off-rate rather than on the on-rate of the ligand–receptor complex [20,22]. For interactions with TNFR1, the LTα mutants exhibited higher k_{off} values compared with the value for wtLTα, whereas the k_{on} values for the LTα mutants were almost same as that for wtLTα. In addition, the bioactivity of wtLTα and LTα mutants was related to k_{off} but not to k_{on}. These data suggest that the LTα mutants interact with TNFR1 by slow dissociation and induce robust signal transduction. In contrast, for interactions with TNFR2, the LTα mutants showed a higher k_{on} than that for wtLTα, whereas the k_{off} values for the LTα mutants was almost same as that for wtLTα. These data indicate that the detailed molecular dissection of ligand-receptor binding kinetics is important for the construction of functional LTα mutants with desired TNFR-mediated bioactivity.

We previously demonstrated that Lys84 of LTα plays a crucial role in the protein's interaction with the main chain of TNFR1 [12]. Here, to explore the role of Lys84 further, we created LTα mutants with Lys84 replaced by Ser84 or Thr84, and found that the mutant with Ser84 showed slower dissociation kinetics and increased bioactivity when compared with wtLTα or the other mutants (Table 5). These results suggest that Lys84 contributes to the TNFR1-mediated bioactivity and the binding kinetics of the TNFR1–LTα interaction. In all three mutants analyzed here, the amino acid Lys at position 28 was changed to Gln (Table 1). Whereas these mutants exhibited increased TNFR1-mediated bioactivity, our previous data showed that a mutant with a K28Q substitution had decreased TNFR1-mediated bioactivity compared with that of wtLTα. Furthermore, mutLT2, which has the Lys at position 39 replaced by Ser, showed slightly increased TNFR2-mediated bioactivity, but a mutant containing the equivalent substitution at the same position showed decreased TNFR2-mediated bioactivity in our previous study [12]. These results suggest

that the sum of the mutations, including those at positions 28 and 39, were responsible for the augmented binding affinities to TNFR1 and TNFR2.

TNFR1 triggers apoptotic caspase signaling following activation of Fas-associated protein with death domain (FADD) [17]. At the same time, triggering of TNFR1 signals induces the anti-apoptotic NFκB cascade following the activation of TNF receptor-associated death domain (TRADD) and TNF receptor-associated factor (TRAF) adaptors [18,19,24]. Active NFκB induces transcription of a set of genes encoding anti-apoptotic proteins [25,26]. Therefore, in many cell types, TNF α has no apoptotic effects due to the parallel triggering by TNF α of a signaling pathway that activates NFκB *via* the TRADD and TRAF adaptors. Here, however, we found that the LTα mutants, which showed augmented bioactivity *via* TNFR1, efficiently induced caspase activation but induced NFκB to the same level as that induced by wtLTα (Figs. 4 and 5). We consider that the slower rate of dissociation of the LTα mutants from TNFR1 was important to the activation of FADD signaling cascade, but not to the activation of TRADD and TRAF adaptors. We speculate that the alteration of the binding mode of LTα mutant to TNFR1 increased the caspase signaling pathway, but not TRADD- and TRAF-mediated NFκB signaling. These findings will facilitate the construction of functional LTα mutants with even higher receptor selectivity and bioactivity in the future.

5. Conclusions

Here, we created highly bioactive LTα mutants with TNFR1-selectivity by using a phage display technique, and we clarified the molecular basis of their augmented TNFR1-mediated bioactivity. A better understanding of the correlation between structure, kinetic behavior, and activity will likely accelerate drug discovery because it will increase awareness of the properties of therapeutic proteins. We suggest that LTα mutants have the potential to be a powerful tool for cancer therapy by combination of direct pro-apoptotic effects of LTα on tumor cells and an enhancement of local/systemic immunity, and that our findings provide valuable information for the construction of even more functional LTα mutants.

Acknowledgements

The authors declare that they have no conflict of interests. This study was supported in part by grants from the Ministry of Health, Labor, and Welfare in Japan; by the Research on Health Sciences focusing on Drug Innovation from the Japan Health Sciences Foundation; and by the Takeda Science Foundation.

References

[1] Neumann B, Luz A, Pfeffer K, Holzmann B. Defective Peyer's patch organogenesis in mice lacking the 55-kD receptor for tumor necrosis factor. J Exp Med 1996;184:259–64.
[2] Kratz A, Campos-Neto A, Hanson MS, Ruddle NH. Chronic inflammation caused by lymphotoxin is lymphoid neogenesis. J Exp Med 1996;183:1461–72.
[3] Koni PA, Sacca R, Lawton P, Browning JL, Ruddle NH, Flavell RA. Distinct roles in lymphoid organogenesis for lymphotoxins alpha and beta revealed in lymphotoxin beta-deficient mice. Immunity 1997;6:491–500.
[4] Schrama D, thor Straten P, Fischer WH, McLellan AD, Brocker EB, Reisfeld RA, et al. Targeting of lymphotoxin-alpha to the tumor elicits an efficient immune response associated with induction of peripheral lymphoid-like tissue. Immunity 2001;14:111–21.
[5] Schrama D, Voigt H, Eggert AO, Xiang R, Zhou H, Schumacher TN, et al. Immunological tumor destruction in a murine melanoma model by targeted LTalpha independent of secondary lymphoid tissue. Cancer Immunol Immunother 2008;57:85–95.
[6] Ryan SM, Mantovani G, Wang X, Haddleton DM, Brayden DJ. Advances in PEGylation of important biotech molecules: delivery aspects. Expert Opin Drug Deliv 2008;5:371–83.
[7] Yamamoto Y, Tsutsumi Y, Yoshioka Y, Nishibata T, Kobayashi K, Okamoto T, et al. Site-specific PEGylation of a lysine-deficient TNF-alpha with full bioactivity. Nat Biotechnol 2003;21:546–52.
[8] Shibata H, Yoshioka Y, Ikemizu S, Kobayashi K, Yamamoto Y, Mukai Y, et al. Functionalization of tumor necrosis factor-alpha using phage display technique and PEGylation improves its antitumor therapeutic window. Clin Cancer Res 2004;10:8293–300.
[9] Narimatsu S, Yoshioka Y, Watanabe H, Masano T, Morishige T, Yao X, et al. Lysine-deficient lymphotoxin-alpha mutant for site-specific PEGylation. Cytokine 2011;56:489–93.
[10] Everaerdt B, Brouckaert P, Shaw A, Fiers W. Four different interleukin-1 species sensitize to the lethal action of tumour necrosis factor. Biochem Biophys Res Commun 1989;163:378–85.
[11] Brouckaert P, Libert C, Everaerdt B, Fiers W. Selective species specificity of tumor necrosis factor for toxicity in the mouse. Lymphokine Cytokine Res 1992;11:193–6.
[12] Yoshioka Y, Watanabe H, Morishige T, Yao X, Ikemizu S, Nagao C, et al. Creation of lysine-deficient mutant lymphotoxin-alpha with receptor selectivity by using a phage display system. Biomaterials 2010;31:1935–43.
[13] Browning JL, Miatkowski K, Sizing I, Griffiths D, Zafari M, Benjamin CD, et al. Signaling through the lymphotoxin beta receptor induces the death of some adenocarcinoma tumor lines. J Exp Med 1996;183:867–78.
[14] Abe Y, Yoshikawa T, Kamada H, Shibata H, Nomura T, Minowa K, et al. Simple and highly sensitive assay system for TNFR2-mediated soluble- and transmembrane-TNF activity. J Immunol Methods 2008;335:71–8.
[15] Nicholls A, Sharp KA, Honig B. Protein folding and association: insights from the interfacial and thermodynamic properties of hydrocarbons. Proteins 1991;11:281–96.
[16] Mizuguchi K, Deane CM, Blundell TL, Johnson MS, Overington JP. JOY: protein sequence-structure representation and analysis. Bioinformatics 1998;14:617–23.
[17] Sheikh MS, Huang Y. Death receptor activation complexes: it takes two to activate TNF receptor 1. Cell Cycle 2003;2:550–2.
[18] Chen G, Goeddel DV. TNF-R1 signaling: a beautiful pathway. Science 2002;296:1634–5.
[19] Magne N, Toillon RA, Bottero V, Didelot C, Houtte PV, Gerard JP, et al. NF-kappaB modulation and ionizing radiation: mechanisms and future directions for cancer treatment. Cancer Lett 2006;231:158–68.
[20] Hlavacek WS, Redondo A, Metzger H, Wofsy C, Goldstein B. Kinetic proofreading models for cell signaling predict ways to escape kinetic proofreading. Proc Nat Acad Sci USA 2001;98:7295–300.
[21] Liu ZJ, Haleem-Smith H, Chen H, Metzger H. Unexpected signals in a system subject to kinetic proofreading. Proc Nat Acad Sci USA 2001;98:7289–94.
[22] Krippner-Heidenreich A, Tubing F, Bryde S, Willi S, Zimmermann G, Scheurich P. Control of receptor-induced signaling complex formation by the kinetics of ligand/receptor interaction. J Biol Chem 2002;277:44155–63.
[23] Torigoe C, Faeder JR, Oliver JM, Goldstein B. Kinetic proofreading of ligand–FcepsilonRI interactions may persist beyond LAT phosphorylation. J Immunol 2007;178:3530–5.
[24] Kim JY, Lee JY, Kim DG, Koo GB, Yu JW, Kim YS. TRADD is critical for resistance to TRAIL-induced cell death through NF-kappaB activation. FEBS Lett 2011;585:2144–50.
[25] Arch RH, Gedrich RW, Thompson CB. Tumor necrosis factor receptor-associated factors (TRAFs) – a family of adapter proteins that regulates life and death. Genes Dev 1998;12:2821–30.
[26] Deveraux QL, Reed JC. IAP family proteins–suppressors of apoptosis. Genes Dev 1999;13:239–52.

Protein Engineering, Design & Selection vol. 26 no. 10 pp. 589–598, 2013
Published online June 5, 2013 doi:10.1093/protein/gzt022

Engineered antibody Fc variant with selectively enhanced FcγRIIb binding over both FcγRIIa^{R131} and FcγRIIa^{H131}

F.Mimoto, H.Katada, S.Kadono, T.Igawa[1], T.Kuramochi, M.Muraoka, Y.Wada, K.Haraya, T.Miyazaki and K.Hattori

Research Division, Chugai Pharmaceutical Co., Ltd., Gotemba, Shizuoka, Japan

[1]To whom correspondence should be addressed.
E-mail: igawatmy@chugai-pharm.co.jp

Received November 22, 2012; revised April 24, 2013; accepted May 8, 2013

Edited by Dario Neri

Engaging inhibitory FcγRIIb by Fc region has been recently reported to be an attractive approach for improving the efficacy of antibody therapeutics. However, the previously reported S267E/L328F variant with enhanced binding affinity to FcγRIIb, also enhances binding affinity to FcγRIIa^{R131} allotype to a similar degree because FcγRIIb and FcγRIIa^{R131} are structurally similar. In this study, we applied comprehensive mutagenesis and structure-guided design based on the crystal structure of the Fc/FcγRIIb complex to identify a novel Fc variant with selectively enhanced FcγRIIb binding over both FcγRIIa^{R131} and FcγRIIa^{H131}. This novel variant has more than 200-fold stronger binding affinity to FcγRIIb than wild-type IgG1, while binding affinity to FcγRIIa^{R131} and FcγRIIa^{H131} is comparable with or lower than wild-type IgG1. This selectivity was achieved by conformational change of the C_H2 domain by mutating Pro to Asp at position 238. Fc variant with increased binding to both FcγRIIb and FcγRIIa induced platelet aggregation and activation in an immune complex form *in vitro* while our novel variant did not. When applied to agonistic anti-CD137 IgG1 antibody, our variant greatly enhanced the agonistic activity. Thus, the selective enhancement of FcγRIIb binding achieved by our Fc variant provides a novel tool for improving the efficacy of antibody therapeutics.

Keywords: antibody engineering/FcγRIIb/Fc engineering/inhibitory FcγR/platelet activation

Introduction

IgG-based monoclonal antibodies (mAbs) have become important therapeutic options for numerous diseases (Brekke and Sandlie, 2003; Maggon, 2007). Fcγ receptors (FcγR)-dependent cytotoxicity plays an important role in the antitumor activity of mAbs for cancer immunotherapy (Nimmerjahn and Ravetch, 2012).

Several works describe engineering the Fc region to enhance the effector function of mAbs by increasing the binding affinity for active FcγRs (FcγRIa, FcγRIIa and FcγRIIIa) with amino acid substitutions. For example, antibodies engineered to have increased binding affinity for FcγRIIIa exhibited superior *in vitro* ADCC activity and *in vivo* antitumor activity compared with wild-type mAbs (Stavenhagen *et al.*, 2007; Zalevsky *et al.*, 2009). In addition to protein engineering, glyco-engineered tumor-specific mAbs with afucosylated N-linked oligosaccharides at Asn297 in the Fc region showed increased binding affinity for human FcγRIIIa and mouse FcγRIV, which resulted in enhancing the therapeutic activity in mouse models (Nimmerjahn and Ravetch, 2005; Mossner *et al.*, 2010).

In contrast to these activating FcγRs that function as immunostimulatory receptors, inhibitory FcγRIIb is reported to function as an immunomodulatory receptor (Li and Ravetch, 2011; White *et al.*, 2011). The inhibitory receptor FcγRIIb is the only IgG Fc receptor expressed on B-cells and plays a critical role in regulating B-cell homeostasis (Heyman, 2003; Nimmerjahn and Ravetch, 2008). Immune complexes (ICs) coengage FcγRIIb and B-cell receptor (BCR) and then selectively suppress B-cells that recognize cognate antigen (Heyman, 2003). FcγRIIb also regulates other B-cell stimulators that amplify B-cell proliferation and differentiation and suppresses the expression of costimulatory molecules (Leibson, 2004; Crowley *et al.*, 2009).

FcγRIIb also plays an inhibitory role in a homeostatic checkpoint of dendritic cells (DCs) for inducing tolerance or immunity by ICs, in contrast to FcγRIIa. While ligation of FcγRIIa led to DC maturation, targeting FcγRIIb alone did not activate DCs (Boruchov *et al.*, 2005). FcγRIIb on DCs induced peripheral tolerance by inhibiting antigenic processing and DC activation to suppress T-cell activation (Desai *et al.*, 2007).

Besides these inhibitory effects of FcγRIIb, several groups have recently reported that FcγRIIb enhances the agonistic activity of anti-tumor necrosis factor receptor (TNFR) superfamily antibody by working as a scaffold (White *et al.*, 2013). Proliferation of antigen-specific T-cells induced by anti-CD40 antibodies was abrogated in FcγRIIb-deficient mice (White *et al.*, 2011; Li and Ravetch, 2012). Anti-death receptor 5 (DR5) agonist antibody also required FcγRIIb to exert its agonistic activity and initiate apoptosis in lymphoma cells (Wilson *et al.*, 2011). The FcγRIIb-expressing cells are considered to work as a scaffold to efficiently cross-link anti-CD40 or DR5 antibodies bound to target cells via FcγRIIb.

In order to exploit these properties, engineering Fc region to increase the binding affinity to FcγRIIb is considered to be a promising approach. Introducing S267E/L328F substitutions

into the Fc region of human IgG1 increased the binding affinity to FcγRIIb 430-fold without increasing that to FcγRI, FcγRIIa^{H131} or FcγRIIIa (Chu *et al.*, 2008). Anti-CD19 antibody with the Fc promoted suppression of B-cell activation and proliferation in SLE mouse model by coengaging FcγRIIb with BCR (Horton *et al.*, 2011). Recent reports noted that anti-IgE antibody with S267E/L328F Fc variant reduced the production of IgE *in vivo* (Chu *et al.*, 2012) and that the Fcε domain fused with S267E/L328F Fc variant suppressed degranulation and calcium mobilization of mast cells (Cemerski *et al.*, 2012). Moreover, agonistic antibodies against CD40 or DR5 showed more potent agonistic activity *in vivo* with enhanced FcγRIIb binding (Li and Ravetch, 2011, 2012). These reports clearly demonstrate that engineered Fc with enhanced binding to FcγRIIb has various therapeutic applications. However, it was reported that S267E/L328F substitutions also enhanced the binding to one of the FcγRIIa allotypes, FcγRIIa^{R131}, to a level similar to the binding to FcγRIIb (Smith *et al.*, 2012). Therefore, when applying the substitutions to mAb therapeutics, the consequence of increasing the binding to FcγRIIa should be considered.

It is reported that a high incidence of thromboembolic complication was observed in patients treated with anti-CD154 or anti-VEGF antibody in clinical settings (Boumpas *et al.*, 2003; Scappaticci *et al.*, 2007). The ICs composing of these antibodies and the antigens activated platelets and induced thrombosis in human FcγRIIa transgenic mice by crosslinking FcγRIIa expressed on the platelets (Meyer *et al.*, 2009; Robles-Carrillo *et al.*, 2010). Moreover, intravenous immunoglobulins also induced FcγRIIa-mediated platelet aggregation *in vitro* (Pollreisz *et al.*, 2008). These results demonstrate that even wild-type IgG1 generally has a potential risk of inducing thromboembolism through an FcγRIIa-dependent mechanism, suggesting that this risk could be increased if the binding to FcγRIIa is enhanced. Therefore, considering the therapeutic applications, antibody with selectively enhanced binding to FcγRIIb relative to both FcγRIIa^{R131} and FcγRIIa^{H131} is preferred.

In this work, we investigated antibodies with selectively enhanced binding to FcγRIIb over both FcγRIIa^{R131} and FcγRIIa^{H131}. We screened a large set of single substituted variants of human IgG1 for binding to human FcγRs and found a distinct variant that distinguishes FcγRIIb from both FcγRIIa allotypes. We solved its crystal structure in complex with human FcγRIIb and elucidated the structural recognition mechanism by which it recognizes FcγRIIb over both FcγRIIa allotypes. In order to improve its FcγRIIb binding, we conducted further optimization and identified a novel antibody variant with over 200-fold more enhanced binding to FcγRIIb without increasing the binding to either FcγRIIa allotype. Structural analysis of this variant revealed the mechanism of the improved binding to FcγRIIb. We also report that antibody that also has enhanced binding to FcγRIIa is more likely to activate platelets and induce aggregation and would have a shorter *in vivo* half-life compared to wild-type IgG1. We also confirmed that this variant enhanced the agonistic activity of anti-CD137 antibody *in vitro*. Our results indicate that the novel Fc variant with purely selectively enhanced binding to FcγRIIb is applicable to a broad range of therapeutic antibodies, since it avoids increasing the potential to activate or aggregate platelets and to have rapid clearance *in vivo*.

Materials and methods

Preparation of IgG1 variants

IgG1 variants used in the experiments were expressed transiently in FreeStyle™ 293F cells transfected with plasmids encoding heavy and light chain and purified from culture supernatants using protein A. Site-directed mutagenesis of the Fc region was performed using QuikChange Site-Directed Mutagenesis Kit (Stratagene) or In-Fusion HD Cloning Kit (Clontech).

Construction, expression and purification of FcγRs

The genes encoding the extracellular region of human FcγRs were synthesized based on the sequence information obtained from the National Center for Biotechnology Information. FcγRs were fused with 6× His-tag at their C-terminus. Vectors containing FcγRs were transfected into FreeStyle™ 293F cells. The receptors were purified from the harvested culture supernatants by using ion exchange chromatography, nickel affinity chromatography and size exclusion chromatography.

Binding and affinity analysis for human FcγRs by surface plasmon resonance (SPR)

The interaction of antibody variants with FcγRs was monitored using Biacore instruments (GE Healthcare), as previously described (Richards *et al.*, 2008). Antibody variants were captured on the CM5 sensor chip (GE Healthcare) on which antigen peptide or protein A/G (Thermo Scientific) was immobilized, followed by injection of FcγRs. The binding of each variant to each FcγR was normalized by the captured amount of antibody on the sensor chip and was expressed as a percentage of that of IgG1. Kinetic analysis was performed by global fitting of binding data with a 1 : 1 Langmuir binding model using Biacore Evaluation Software (GE Healthcare).

Crystalization, data collection and structure determination of the complex of Fc fragment of human IgG1 with P238D substitution, Fc(P238D) and FcγRIIb

Crystals were obtained by 1 : 1 mixing of protein complex (10 mg/ml) with 0.1 M Bis-Tris pH6.5, 0.2 M ammonium acetate, 2.7% (w/v) D-galactose, 17% PEG3350 in sitting drop vapor diffusion setups at 20°C. For data collection, crystals were flash frozen at 95 K in precipitant solution containing 22.5% ethylene glycol. Diffraction data to 2.6 Å were collected using the Photon Factory beamline BL-1A. Data were processed with Xia2 (Winter, 2010), XDS Package (Kabsch, 2010) and Scala (Evans, 2006). The structure was determined by molecular replacement with PHASER (McCoy *et al.*, 2007) using Fc part of Fc(IgG1)/FcγRIIIa structure (PDB ID: 3SGJ) and FcγRIIb structure (PDB ID: 2FCB) as search models. The asymmetric unit was formed by a single 1 : 1 complex. A model was built with the program Coot (Emsley *et al.*, 2010) and refined with the program REFMAC5 (Murshudov *et al.*, 2011).

Crystalization, data collection and structure determination of the complex of Fc fragment of V12 variant, Fc(V12) and FcγRIIb

Crystals were obtained by 1 : 1 mixing of protein complex (10 mg/ml) with 0.1 M Bis-Tris pH6.5, 0.2 M potassium phosphate dibasic, 19% PEG3350 in hanging drop vapor diffusion

setups at 20°C. For data collection, crystals were flash frozen at 95 K in precipitant solution containing 20% ethylene glycol. Diffraction data to 2.86 Å were collected at the SPring-8 beamline BL-32XU. After data processing and structure determination by molecular replacement using Fc(P238D)/FcγRIIb structure, a model was built with the program Coot and refined with the program REFMAC5. The asymmetric unit was formed by a single 1 : 1 complex.

Data collection and refinement statistics of both crystals are summarized in Supplementary Table S1. All graphical presentations were prepared with PyMOL (DeLano, 2002).

Preparation of Fc fragment and FcγRIIb complexes

We cloned recombinant Fc fragments corresponding to the heavy chain residues from 216 (EU numbering) to C-terminus for the crystallization. Cys 220 was replaced with Ser so that the free cysteine would not make disulfide bonds. FcγRIIb expressed by FreeStyle™ 293F cells in the presence of the mannosidase I inhibitor, kifunensine, was purified and treated with endoglycosidase F1 fused with glutathione *S*-transferase for deglycosylation as described previously to minimize the heterogeneity of the oligosaccharide (Grueninger-Leitch *et al.*, 1996). The complexes of Fc fragment and the deglycosylated FcγRIIb were prepared by mixing Fc fragment with a little excess of the deglycosylated FcγRIIb, and purified by size exclusion chromatography.

Thermal shift assay

Melting temperature (T_M) of the C_H2 region was measured as previously described (He *et al.*, 2010). The SYPRO orange dye (Invitrogen) was added to 0.1 mg/ml protein solutions at a final dilution of 1 : 500. Fluorescence measurements were employed using a real-time polymerase chain reaction instrument, Rotor-Gene Q (QIAGEN). The temperature was increased from 30 to 99°C at a heating rate of 4°C/min.

Stability study of high concentration antibodies

Antibodies were concentrated to 100 mg/ml in a histidine buffer (20 mM histidine, 150 mM NaCl, pH6.0) by ultrafiltration (Millipore). The solutions were stored at 25°C to assess the stability of the antibodies. High-molecular-weight (HMW) species were analyzed with TSK-GEL G3000SWXL column (TOSOH) by size exclusion high-performance liquid chromatography at initial time point and after 4 weeks. The mobile phase contained 300 mM NaCl in 50 mM phosphate at pH7.0. The percentage of HMW species peak in total protein peak area was calculated using Empower Waters software.

Binding affinity analysis of antibodies for human FcRn

Recombinant, soluble human FcRn (hFcRn) was expressed in HEK293 cells and prepared as described previously (Dall'Acqua *et al.*, 2006). The interaction of soluble hFcRn was monitored as described previously (Igawa *et al.*, 2010).

Pharmacokinetic studies of monoclonal antibodies in hFcRn transgenic mouse

Anti-human interleukin-6 receptor (hIL-6R) IgG1 or V12 variant was administered to human FcRn (hFcRn) transgenic mice (B6.mFcRn$^{-/-}$ hFCRN Tg32 B6.Cg-Fcgrt<tm1Dcr> Tg(FCGRT)32Dcr; Jackson Laboratories) by single intravenous injection together with 1 g/kg Sanglopor (CSL Behring K.K.) to mimic endogenous IgG in human. Blood samples were collected. The concentration of each antibody was determined by capture with anti-idiotype antibody (in-house), followed by addition of hIL-6R and biotinylated anti-hIL-6R antibody (R&D Systems) and detected by Streptavidin-Poly HRP80. The half-life was calculated from the plasma concentration–time data using non-compartmental analysis with WinNonlin Professional software (Pharsight).

Platelet aggregation and activation study using washed platelets

Fresh blood from healthy volunteers whose FcγRIIa genotype is R/R or H/H was anticoagulated with 0.5 ml of 3.8% sodium citric acid–citrate in blood collection tubes. Platelet-rich plasma (PRP) was obtained by centrifuging at 200 *g* for 15 min and then removing the supernatant. PRP was washed in modified Tyrode buffer (137 mM NaCl, 2.7 mM KCl, 12 mM $NaHCO_3$, 0.42 mM NaH_2PO_4, 2 mM $MgCl_2$, 5 mM HEPES, 5.55 mM dextrose, 0.35% bovine serum albumin) with 1.5 U/ml apyrase and resuspended at a concentration of 3×10^8/ml in modified Tyrode buffer. Washed platelets were then incubated with preformed IC for 5 min. The Preformed IC was prepared by mixing the anti-IgE mAb having different Fc variants (200 μg/ml) with its antigen (229 μg/ml), human IgE, at a molar ratio 1 : 1. Five minutes after the incubation, 30 μM ADP was added to induce the first wave of platelet aggregation. Platelet aggregation was measured by an aggregometer (MCM Hema Tracer 712; MC Medical) at 37°C with stirring at 1000 rpm.

Cells and reagents

CTLL-2 cells (mouse T lymphocyte cell line, No.RCB0637) were provided by the RIKEN BRC through the National Bio-Resource Project of the MEXT, Japan. Raji cells (human Burkitt's lymphoma cell line, ATCC No.CCL-86) were purchased from the American Type Culture Collection. Both cell lines were cultured in RPMI 1640 medium (Nacalai tesque), supplemented with 10% heat-inactivated foetal bovine serum (Bovogen). The culture medium for CTLL-2 was supplemented with 10 ng/ml recombinant mouse interleukin (IL)-2 (PeproTech). The culture medium for Raji cells was supplemented with 10 mM HEPES, 1 mM sodium pyruvate (Nacalai tesque), 4.5 g/l D-glucose, 1.5 g/l sodium bicarbonate (Sigma-Aldrich).

Flow cytometry analysis of CD137 expression

To analyze mouse CD137 expression on CTLL-2 cells, anti-mouse CD137 clone 1D8 variable region fused with the Fc domain of human IgG1 (Shuford *et al.*, 1997) or human IgG1 isotype control (Alexis, Lausen) was applied. Goat F(ab')2 anti-human IgG-FITC #732596 (Beckman Coulter) was used as the detection antibody. Cell Lab Quanta SC MPL system (Beckman Coulter) was used for cell acquisition and data analysis was conducted using FlowJo software (Tree Star Inc.).

Measurement of T-cell activation by anti-CD137 antibody by cytokine production

CTLL-2 cells (2×10^5/mL) and Raji cells (2×10^5/ml) were co-cultured in RPMI 1640 medium supplemented with 10% heat-inactivated foetal bovine serum (Bovogen), 10 ng/ml mouse IL-2 (PeproTech), 10 ng/ml phorbol 12-myristate 13-acetate, 0.5 μg/ml ionomycin (Sigma-Aldrich). The cells were treated with 3 μg/ml anti-CD137 antibodies with

different Fc (Fc of human IgG1, S267E/L328F or V12 variant) for 24 h at 37°C, 5% CO_2. Mouse interferon (IFN)-γ concentration in the cultured medium was determined by ELISA system (PeproTech), according to the manufacturer's protocol.

Results

Screening and characterization of variants to selectively enhance FcγRIIb binding by comprehensive mutagenesis

We screened a large set of over 500 variants prepared by replacing each of about 30 residues in the lower hinge and C_H2 region with every naturally occurring amino acid except for cysteine, for binding to human FcγRIIa^{H131}, FcγRIIa^{R131} and FcγRIIb in order to identify substitutions that selectively enhance FcγRIIb binding relative to both FcγRIIa allotypes. The effect of each substitution on the binding to FcγRIIa^{R131}, FcγRIIa^{H131} and FcγRIIb is compared in Fig. 1A and B. Only two substitutions, P238D and L328E, were found to enhance FcγRIIb binding while decreasing the binding to both FcγRIIa allotypes, although previously reported S267E and L328F increased both binding.

We compared the dissociation constant (K_D) of wild-type human IgG1, P238D variant and L328E variant (Supplementary Table S2) and the changes in affinity from IgG1 are shown in Fig. 2. Both P238D and L328E variants enhanced affinity to FcγRIIb, while reduced affinity to both FcγRIIa^{R131} and FcγRIIa^{H131}. P238D variant reduced the affinity for all the active FcγRs and enhanced that for FcγRIIb more significantly than L328E variant.

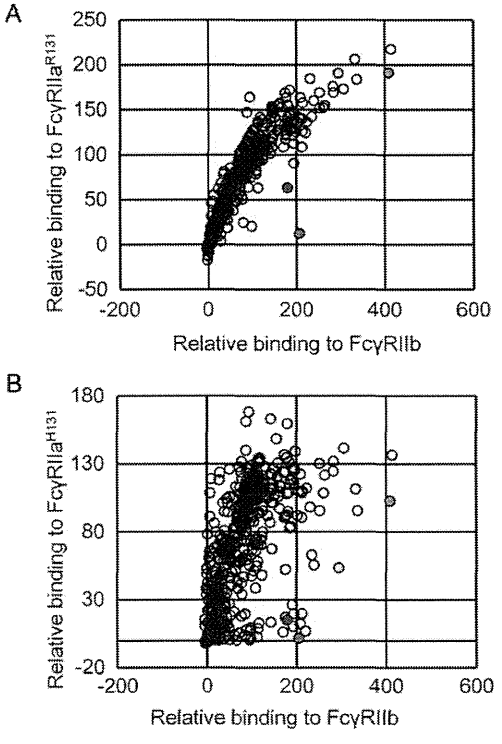

Fig. 1. Comprehensive mutagenesis of the lower hinge and C_H2 region. Binding affinity for FcγRIIa^{R131}, FcγRIIa^{H131} and FcγRIIb was evaluated. The binding to FcγRIIa^{R131}, FcγRIIa^{H131} or FcγRIIb of template antibody was normalized to 100. The binding to FcγRIIa^{R131} and FcγRIIb is shown in panel **A** and the binding to FcγRIIa^{H131} and FcγRIIb is shown in panel **B**. Novel substitutions to selectively improve FcγRIIb binding, L328E and P238D, are indicated in blue and red, respectively. Previously reported substitutions, S267E and L328F, to improve FcγRIIb but also FcγRIIa^{R131} binding are indicated in green and yellow, respectively.

Crystal structure of the FcγRIIb complex with IgG1 Fc fragment with P238D

Fc(P238D) bound to FcγRIIb in an asymmetric fashion between the two C_H2 domains (C_H-A and C_H-B) like previously reported Fc(IgG1) and FcγR complexes. In Fig. 3A, the overall structure of Fc(P238D)/FcγRIIb was compared with known Fc(IgG1)/FcγRIIa^{R131} (PDB ID: 3RY6) (Ramsland *et al.*, 2011). Despite the high-sequence homology between FcγRIIb and FcγRIIa^{R131} (Supplementary Fig. S1), the domain arrangement of C_H2-B in Fc(P238D)-FcγRIIb interface was different from that in Fc(IgG1)/FcγRIIa^{R131}.

Structural comparisons of both C_H2 domains with those of Fc(IgG1) complexed with FcγRIIa^{R131} revealed conformational changes of loops around position 238 in both C_H2 domains (Fig. 3B and C). Pro238 in wild-type human IgG1 formed an inside hydrophobic core with Val263, Val266, V323, Asn325 and Leu328. On the other hand, Asp238 in P238D variant shifted out of the core and it was exposed to the solvent region. Instead, Leu235 occupied the vacated space which Pro238 occupied in Fc(IgG1), forming another hydrophobic core in C_H2-A, but not in C_H2-B. As a result, there was a large cavity surrounded by Val263, Val266, Val273, Val323, Asn325 and Leu328 in C_H2-B. Asp238 in C_H2-B formed an electrostatic interaction with Lys334 in the same chain.

In the C_H2-A domain, the main chain of Gly237 formed a novel hydrogen bond with Tyr160 of FcγRIIb (Fig. 3B). A weak hydrogen bond between the main chain of Asp238 and the side chain of Thr158 of FcγRIIb was also observed. In addition, the side chain of Asp238 formed van der Waals contacts with the side chain of Thr158 in FcγRIIb. In the C_H2-B domain, the conformation of the loop around Asp270 changed from that of Fc(IgG1) complexed with FcγRIIa^{R131}, and Asp270 formed a salt bridge with Arg131 of FcγRIIb (Fig. 3C).

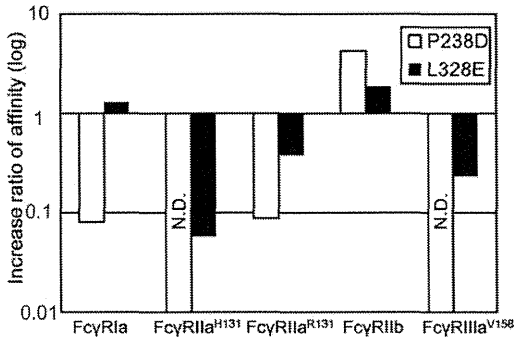

Fig. 2. Affinity ratio of Fc variants identified by comprehensive mutagenesis for all the human FcγRs. The binding of P238D variant to FcγRIIa^{H131} and FcγRIIIa^{V158} and that of L328E variant to FcγRIIa^{H131} were not detected. Affinity ratio was calculated by the equation, K_D (IgG1)/K_D (Fc variant).